

Low-lying collective states in $^{124-132}\text{Ba}$ in the framework of the general collective model

P. Petkov,^{1,2} A. Dewald,¹ and W. Andrejtscheff²

¹*Institut für Kernphysik, Universität zu Köln, D-50937 Köln, Germany*

²*Bulgarian Academy of Sciences, Institute for Nuclear Research and Nuclear Energy, 1784 Sofia, Bulgaria*

(Received 26 July 1994; revised manuscript received 17 January 1995)

The general collective (or Frankfurt) model (GCM) is applied to the barium isotopes with $A=124-132$. A good description of the experimental level schemes is obtained and in particular, the staggering effect in the quasi- γ bands of these nuclei is reproduced. The description of the $E2$ transition strengths is also satisfactory but the deviations observed for specific weak transitions indicate some crudeness in the present quadrupole operator of the model. The comparison of the derived potential energy surfaces with microscopic nuclear shape calculations shows an overall reasonable agreement. The description of the spectroscopic properties is compared to the results obtained in the framework of other collective models used in the $A \approx 130$ mass region. The structure of the GCM wave functions is investigated and correspondences with the quantum numbers of the interacting boson approximation wave functions are considered.

PACS number(s): 21.60.Ev, 21.60.Fw, 21.10.Re, 27.60.+j

I. INTRODUCTION

The continuous accumulation of extensive experimental information on transitional nuclei in the mass region $A \approx 130$ has provided, during the last decades, a natural testing ground for nuclear models with an ever increasing sensitivity. In the present work, we concentrate on the low-lying collective states of some even barium isotopes in an attempt to clarify what nuclear shapes underlay the observed energy spectra and $B(E2)$ transition strengths and how the basic trends in these data are correlated with the shape evolution. For this purpose, the new version (cf. Refs. [1,2] and references therein) of the general collective model (GCM) of Gneuss and Greiner [3] is a suitable tool. In reproducing the nuclear observables, this phenomenological model provides information on the shape described in terms of the intrinsic variables β and γ . Thus, a consistent description of an isotopic chain involves necessarily the corresponding shape evolution visualized by the changes in the collective potential energy $V(\beta, \gamma)$. In particular, the role of nonaxial contributions to $V(\beta, \gamma)$ can be investigated in the framework of the model. The separation of the kinetic and potential energy terms in the Hamiltonian also allows a sensitivity of the calculations with respect to possible deformation dependence of the collective mass parameters. Another aspect of the investigation is the establishment of relations and comparisons with other collective models which were successfully applied in the $A \approx 130$ region as the $O(6)$ limit of the interacting boson approximation (IBA) [4,5] and its geometrical equivalent [6] the model of Willets and Jean [7] as well as the numerical solutions of a microscopically derived collective Bohr Hamiltonian (cf. Ref. [8] and references therein). In our opinion, detailed discussion of a large quantity of observables confronted to the predictions of different models can be only based on further theoretical work in the spirit, e.g., of

the recent calculations by Dobaczewski and Skalski [9] where the comparison of collective nuclear models starts at their microscopic foundations. Staying on the point of view of the experimentalists, after a brief description of the GCM formalism and the details of the calculations, we turn our attention to the following.

(i) Demonstration of the possibility to use the GCM for the description of the nuclei in the $A \approx 130$ mass region. Such attempts were undertaken in the past [10] but their reliability has been limited by the lack of sufficient data at that time. In Sec. III, we present the calculated spectroscopic properties (level energies, electromagnetic transition strengths) and compare them to the experimental data.

(ii) On the basis of (i), a picture of the shape evolution within the barium isotopes considered is derived and compared to the trends predicted by microscopic calculations.

(iii) Comparisons of the properties of the basic excitations as described by the GCM and the above-mentioned nuclear collective models in emphasizing the effects of the shape evolution deduced. The use of a $U(5)$ basis [11] in the present version of the GCM especially facilitates the establishment of relationships with the IBA [11,12,4]. These considerations are concentrated in Sec. IV where the structure of the GCM wave functions describing the $^{124-132}\text{Ba}$ nuclei is also investigated. A summary and conclusions are given in Sec. V.

II. GCM CALCULATIONS

A. The GCM

In order to facilitate the following discussion we present shortly the collective model developed in Frankfurt [3,13]. More details on its present status can be found in Ref.

[14] and the papers quoted therein. For the description of the computer code used the reader is referred to Ref. [2].

The Hamiltonian \hat{H} of the GCM [3] represents a concrete realization of the general Bohr Hamiltonian (cf., e.g., Ref. [15]) describing the quadrupole oscillations of the nuclear surface. In this approximated realization, $\hat{H}=\hat{T}+V$ is expressed in terms of invariant products of the collective quadrupole variables $\alpha_{2\mu}$ which parametrize the nuclear surface

$$R(\theta, \phi) = R_0 \left(1 + \sum_{\mu} \alpha_{2\mu}^* Y_{2\mu}(\theta, \phi) \right) \quad (1)$$

in the center of mass system and their conjugate momenta $\hat{\pi}_{2\mu}$. The approximation consists of a replacement of the deformation (β - and γ -) dependent mass parameters and inertial functions by constants with the effects of such dependence schematically accounted for by the P_3

term in kinetic energy and in the use of a finite number of terms from the series of the Bohr Hamiltonian in $\alpha_{2\mu}$ and $\hat{\pi}_{2\mu}$. Thereby, the kinetic energy \hat{T} is given by

$$\hat{T} = \frac{1}{2B_2} [\hat{\pi} \times \hat{\pi}]^{[0]} + \frac{P_3}{3} \left\{ [[\hat{\pi} \times \alpha]^{[2]} \times \hat{\pi}]^{[0]} \right\}, \quad (2)$$

where $\{\dots\}$ means the sum over all even permutations of $\hat{\pi}$ and α while B_2 is the common mass parameter. A transformation to the intrinsic (body-fixed) system leads to a formal separation of the rotational and vibrational variables, expressed by the Euler angles and the shape variables (parameters) β and γ , respectively. (We remind the reader that the two intrinsic vibrational variables are related to β and γ via the polar transformation $\alpha_{20}^{\text{intrinsic}} = \beta \cos \gamma$ and $\alpha_{22}^{\text{intrinsic}} = \alpha_{2-2}^{\text{intrinsic}} = \beta \sin \gamma / \sqrt{2}$ whereas $\alpha_{21}^{\text{intrinsic}} = \alpha_{2-1}^{\text{intrinsic}} = 0$.) The potential energy V represents a polynomial expansion in α containing all independent terms up to sixth order. In the intrinsic frame, it reads

$$V(\beta, \gamma) = \frac{1}{\sqrt{5}} C_2 \beta^2 - \sqrt{\frac{2}{35}} C_3 \beta^3 \cos 3\gamma + \frac{1}{5} C_4 \beta^4 - \sqrt{\frac{2}{175}} C_5 \beta^5 \cos 3\gamma + \frac{2}{35} C_6 \beta^6 \cos^2 3\gamma + \frac{1}{5\sqrt{5}} D_6 \beta^6 = V_S(\beta) + V_{PO}(\beta, \gamma) + V_{NA}(\beta, \gamma). \quad (3)$$

The eight constants B_2 , P_3 , C_k ($k=2-6$), and D_6 are treated as adjustable parameters which have to be determined from the best fit to the experimental data [level energies, $B(E2)$ transition strengths, and quadrupole moments]. The potential energy surfaces (PES's) corresponding to different nuclear shapes, spherical, prolate, oblate, triaxial, etc., are parametrized by C_k and D_6 . Roughly speaking, the C_2 , C_4 , and D_6 terms describe the γ -independent features of the PES. They form the contribution $V_S(\beta)$ in Eq. (3). The C_3 and C_5 terms are responsible for the prolate-oblate (PO) energy differences in the PES and are represented by $V_{PO}(\beta, \gamma)$. The C_6 term [i.e., $V_{NA}(\beta, \gamma)$] is symmetric about the $\gamma=30^\circ$ axis and therefore can be used for the generation of nonaxial shapes (alone or in combination with other terms). It should be noticed that the actual independent parameters defining the PES are physical quantities as the position of the minimum (or minima), the depth and stiffness in the β - γ plane around a minimum, etc. When mathematically expressed via equations involving the potential $V(\beta, \gamma)$ and its derivatives, they determine the corresponding set of parameters C_k and D_6 . Therefore, limitations imposed on the above physical quantities (obtained, e.g., from microscopic calculations or an empirical systematics) are equivalent to a significant reduction of the freedom in varying the parameters describing the PES.

The Hamiltonian is diagonalized in the basis of the five-dimensional quadrupole oscillator

$$|\nu\lambda\mu IM\rangle = \sum_{K=0,2,\dots}^I F_{(\nu-\lambda)/2}^\lambda(\beta) \Phi_K^{\lambda\mu I}(\gamma) \times [D_{MK}^I(\Omega) + (-)^I D_{M-K}^{I*}(\Omega)], \quad (4)$$

where the $D_{MK}^I(\Omega)$ are the Wigner functions which project to the laboratory system the different K components of the intrinsic vibrational wave function factorized into β - and γ -dependent parts. (Detailed expressions for $F_{(\nu-\lambda)/2}^\lambda(\beta)$ and $\Phi_K^{\lambda\mu I}(\gamma)$ are given in Ref. [13].) The quantum numbers have the following physical meaning. The number of quadrupole phonons is denoted by ν , λ is the number of phonons which are not coupled pairwise to angular momentum $L=0$, and μ is the number of phonon triplets coupled to $L=0$. The number of nodes in β of the basis wave function [Eq. (4)] is given by $n_\beta = (\nu-\lambda)/2$. The maximal number of phonons $N_{\text{ph}}^{\text{max}} = 30$ used in the code [2] ensures a convergence in the range of angular momenta of interest for the present work ($I \leq 8 \hbar$).

The calculation of $E2$ matrix elements is performed using the quadrupole operator

$$\hat{Q}_{2\mu} = \frac{3ZR_0^2}{4\pi} \left(\alpha_{2\mu} - \frac{10}{\sqrt{70}\pi} [\alpha \times \alpha]_{2\mu} \right) = \hat{Q}_{2\mu}^{(1)} + \hat{Q}_{2\mu}^{(2)} \quad (5)$$

obtained by averaging $r^2 Y_{2m}(\theta, \phi)$ over the nuclear volume where terms of third and higher orders in β are neglected (for more details see, e.g., Ref. [13]). The selection rules of the operators $\hat{Q}_{2\mu}^{(1)}$ and $\hat{Q}_{2\mu}^{(2)}$ are $\Delta\nu=\pm 1$, $\Delta\lambda=\pm 1$, and $\Delta\nu=0, \pm 2$, $\Delta\lambda=0, \pm 2$, respectively. We used a value of $R_0 = 1.15A^{1/3}$ fm which is between $R_0 = 1.1A^{1/3}$ fm as originally implemented in the code [2] and the more commonly used value of $R_0 = 1.2A^{1/3}$ fm.

Finally, we mention some additional features incorporated by us in the original code [2] which are based on

the knowledge of the wave functions obtained after the diagonalization

$$|IM\rho\rangle = \sum_{\nu\lambda\mu} A_{\nu\lambda\mu}^{I\rho} |\nu\lambda\mu IM\rangle, \quad (6)$$

where ρ labels the different eigenstates with the same angular momentum I . Thus, for each state of interest $|I\rho\rangle$ the expectation values $\langle I\rho | \beta^2 | I\rho\rangle$ and $\langle I\rho | \beta^3 \cos 3\gamma | I\rho\rangle$ are calculated which yield direct information on $\beta_{\text{rms}} = \sqrt{\langle \beta^2 \rangle}$ and the average γ defined by $\langle \gamma \rangle = \frac{1}{3} \arccos(\langle \beta^3 \cos(3\gamma) \rangle / \beta_{\text{rms}}^3)$. The widths σ_β and σ_γ of the distributions represented by the wave functions are determined according to the formulas given in Ref. [8]. The frequency distributions of the quantum numbers labeling the basis states [Eq. (4)] can also be calculated. For example, the distribution of the number of phonons ν is given by

$$F_\nu^{I\rho} = \sum_{\lambda\mu} \left(A_{\nu\lambda\mu}^{I\rho} \right)^2 \quad (7)$$

and the expectation value of ν (i.e., the mean number of phonons) reads

$$\langle I\rho | \nu | I\rho \rangle = \sum_\nu F_\nu^{I\rho} \nu. \quad (8)$$

B. Phenomenological aspects of the data and details of the calculations

Phenomenological data trends. The collective states of interest for the present study can be divided into two groups. On the one hand, these are the states belonging to ground-state band (g.s.b.) and the quasi-gamma band up to spin $I = 8\hbar$. [For the sake of simplicity, hereafter we use γ band instead of quasi-gamma band as it is in the terminology introduced by Sakai (cf., e.g., Ref. [16].)] The second group is represented by the recently established low-lying bands based on $I^\pi=0^+$ and $I^\pi=4^+$ states in $^{124-130}\text{Ba}$ (cf. Refs. [17,18] and references therein as well as Ref. [19] for ^{124}Ba). An overview of the bands of interest along the isotopic chain is shown in Fig. 1. Empirically, the main ingredients of the collective motion at low spin are well known in the investigated nuclei. These are the γ degree of freedom [manifested by the effects of γ softness and (effective) triaxiality] and the gradual stabilization of rotational-like structure when approaching the neutron midshell around ^{122}Ba . In Fig. 1, the general trend of increased quadrupole deformation characterizing the lighter isotopes can be deduced, e.g., from the increase of the ratio $E(4_1^+)/E(2_1^+)$ when the mass number A decreases. The importance of the γ degree of freedom is illustrated by the low-lying 2_2^+ level whose energy position is remarkably constant in the nuclei considered. The closeness of the 2_2^+ level to the 4_1^+ one (especially at $A \geq 130$) as well as the characteristic staggering [$E(I_{\text{even}}) - E(I_{\text{even}} - 1) < E(I_{\text{even}} - 1) - E(I_{\text{even}} - 2)$] of the level energies in the γ -band point at a significant γ softness of the collective potential. The staggering effect

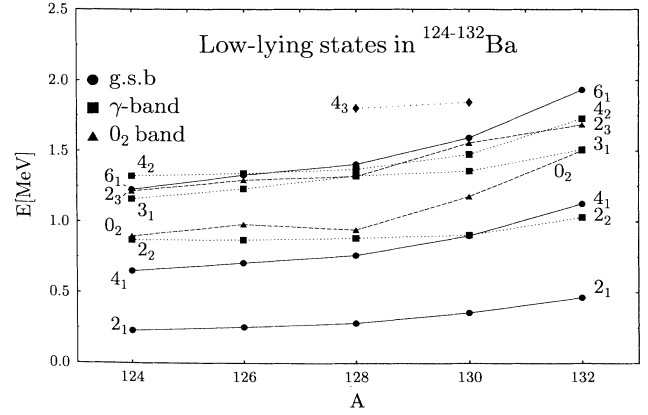


FIG. 1. Excitation energies (relative to that of the 0_1^+ ground state) of the experimental low-lying collective states with positive parity (labeled by spin I) in $^{124-132}\text{Ba}$. Experimental data are taken from ^{124}Ba [19,20], ^{126}Ba [21,22], ^{128}Ba [23,22], ^{130}Ba [18,24], and ^{132}Ba [25,26]. Levels with higher spin belonging to the g.s.b. and γ band are shown in Fig. 3.

is especially pronounced in ^{128}Ba . Further support for this picture is given by the recently [17,18] established 4_3^+ levels in $^{128-130}\text{Ba}$ which can be associated with a “double” γ excitation. Their energies are given in both nuclei within some 30 keV by twice the energy of the 2_2^+ state. The decay patterns are also consistent with such an interpretation. From a geometrical point of view, all these features favor the use of a model which incorporates the γ soft rotor suggested by Willets and Jean [7]. However, the model description should include some degree of prolate-oblate shape difference and/or triaxiality necessary for lifting the degeneracy of the theoretical multiplets labeled by the seniority λ and the number of nodes n_β of the wave function in the β direction. For instance, the first family of excited states of the γ soft rotor are characterized by $n_\beta=0$ and the multiplets are given by $I = 0$ for $\lambda = 0$; $I = 2$ for $\lambda = 1$; $I = 2, 4$ for $\lambda = 2$; $I = 0, 3, 4, 6$ for $\lambda = 3$; $I = 2, 4, 5, 6, 8$ for $\lambda = 4$, etc. An inspection of Fig. 1 suggests that $^{130-132}\text{Ba}$ are good candidates for such a description. As pointed out by Rohozinski *et al.* [27], the barium nuclei with $A < 130$ present difficulties to γ soft models because the relative increase of the level energies in the ground-state band is faster than the theoretical upper limit when the deviation from a γ -independent potential is treated only as a small perturbation. The recently established 0_2^+ states in $^{124-128}\text{Ba}$ add new aspects to the experimental systematics. The closeness of their excitation energies to those of the 2_2^+ and 4_1^+ states certainly indicate a more complex behaviour of the potential in both γ and β directions. It should be mentioned that the consideration of other observables as, e.g., the $B(E2)$ strengths in the g.s.b. do not support a vibrational character of the light barium isotopes as it may be suggested by the existence of the $I = 0_2, 2_2, 4_1$ level group. In our opinion, some caution has to be kept in a model description of the 0_2^+ states in $^{124-128}\text{Ba}$ as collective ones unless complementary data as, e.g., absolute experimental $B(E2)$ values are available. We note also that among all levels dis-

played in Fig. 1 the relative energy position of the 0_2^+ level undergoes the most impressive evolution indicating the occurrence of shape changes at $A = 130$.

Fitting procedure. The above general observations suggest the class of potentials suitable for a quantitative description of the transitional barium isotopes with $124 \leq A \leq 132$. Thereby, the existence of a minimum at $\beta \neq 0$ was assumed. A rough orientation for its position β_{\min} is provided by the local systematics [28] of $B(E2, 2_1^+ \rightarrow 0_1^+)$ values. Also, the observed effects of γ softness imply potentials with relatively small prolate-oblate energy difference. With these general initial conditions and taking into account the physical role of the different terms in $V(\beta, \gamma)$ (cf. Sec. II A), we tried to obtain a consistent description of the experimental quantities in keeping at minimum the number of the active potential parameters. The depth of the potential and the position $(\beta_{\min}, \gamma_{\min})$ of its minimum were adjusted mainly by the fit of the level energies and, wherever such data are available, by the reproduction of the $B(E2)$ strengths for consecutive transitions within the ground-state band. Special interest was paid to the position and level spacing of the γ band. In principle, the observed gross features of the data could be described by using the minimum of three potential parameters, e.g., C_2 , C_3 , and C_4 as well as the mass parameter B_2 which compresses (expands) the

band structures when it increases (decreases). However, it turned out that two more terms in the Hamiltonian have to play an active role in reproducing the γ -band energy spacings. These are the anharmonicity term in the kinetic energy \hat{T} (parametrized by P_3) and the nonaxial term (parametrized by C_6) in $V(\beta, \gamma)$. Moreover, they were also necessary to lower the position of the first excited 0^+ state in $^{124-128}\text{Ba}$. Some improvement of the description of the level energies could be also realized by using the C_5 and D_6 terms and their interplay with the terms with similar dependence on γ but proportional to lower powers of β . The latter effect may be considered as an indication for a more complex dependence of the potential on β . The $B(E2)$ transition strengths were fitted in a second stage of the procedure when the reproduction of the energies was considered as satisfactory. Then, the parameters of the Hamiltonian were adjusted to reproduce the experimental $B(E2, 2_1^+ \rightarrow 0_1^+)$ values. Finally, the description of other $B(E2)$ values was improved (if possible) by allowing slight modifications of the parameters derived heretofore.

The potentials $V(\beta, \gamma)$ obtained are presented in Fig. 2. Their parameters as well as the mass parameters B_2 and P_3 are listed in Table I where some of the physical characteristics of the potentials are also displayed. On the first glance, one could expect a smooth behavior of the

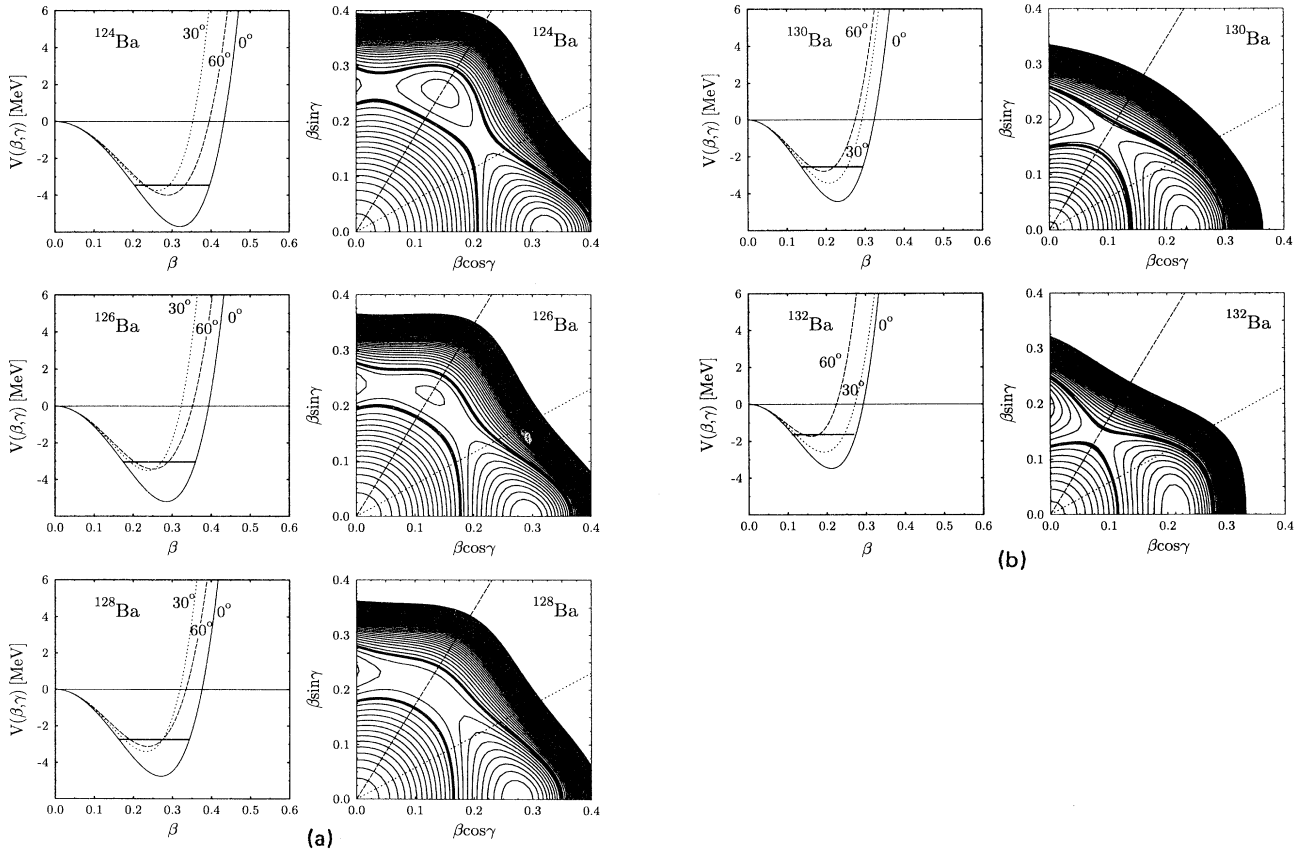


FIG. 2. (a) PES of $^{124-128}\text{Ba}$. To the left, the projections of the potential $V(\beta, \gamma)$ at $\gamma=0^\circ, 30^\circ$, and 60° are shown. On the right-hand part, PES contours differing by 200 keV are displayed. The absolute ground-state energy is indicated by a horizontal line on the l.h.s. plots and by a thicker contour on the r.h.s. plots. See also text. (b) The same as in (a) for $^{130-132}\text{Ba}$.

TABLE I. Parameters of the GCM Hamiltonian used in the present work. The only purpose of presenting their numerical values with a large number of significant digits is to ensure a reproducibility of the calculations. Some physical characteristics of the potentials are also displayed: the depth V_{\min} and the position β_{\min} of the absolute minimum ($\gamma_{\min} \approx 0$ in all cases considered), the PO difference $V_{\text{PO}}^{0^\circ-60^\circ} = \min[V(\beta, 60^\circ)] - \min[V(\beta, 0^\circ)]$ as well as the potential energy differences $V_{0^\circ-30^\circ} = \min[V(\beta, 30^\circ)] - \min[V(\beta, 0^\circ)]$ and $V_{30^\circ-60^\circ} = \min[V(\beta, 60^\circ)] - \min[V(\beta, 30^\circ)]$. The potential parameters, depths, and energy differences are given in MeV.

	^{124}Ba	^{126}Ba	^{128}Ba	^{130}Ba	^{132}Ba
B_2 (10^{-42} MeV s 2)	46.91602	53.8611	56.42193	62.70904	57.933
P_3 (10^{42} MeV $^{-1}$ s $^{-2}$)	-0.13	-0.118	-0.107141	-0.107602	-0.125873
C_2	-209.0632	-252.7933	-263.6945	-352.6598	-314.2383
C_3	135.8335	220.6479	248.7190	362.6218	442.1007
C_4	1708.726	3449.529	4323.475	8848.212	9517.914
C_5	-229.18361	-946.7563	-1371.759	-86.12527	8525.92
C_6	-36499.49	-50421.41	-41041.91	-15557.86	74370.15
D_6	36499.49	41910.09	32030.03	10191.77	-546.2191
V_{\min}	-5.7	-5.2	-4.8	-4.4	-3.5
β_{\min}	0.320	0.286	0.270	0.230	0.212
$V_{\text{PO}}^{0^\circ-60^\circ}$	1.7	1.8	1.6	1.6	1.7
$V_{0^\circ-30^\circ}$	2.0	1.7	1.4	1.0	1.0
$V_{30^\circ-60^\circ}$	-0.3	0.1	0.3	0.7	0.8

potential parameters throughout the isotopic chain and therefore large variations in their values could seem a bit surprising (as, e.g., in the case of C_5 , C_6 , and D_6 at $A \geq 128$). However, only a smooth behavior of the potentials and their physical characteristics (position of the minimum, depth, stiffness around the minimum in the β - γ plane, etc.) is of importance for the physics (shape evolution and accompanying changes in the spectroscopic properties). The latter smoothness can be easily deduced by inspecting the potentials $V(\beta, \gamma)$ presented in Fig. 2. We note also that a scale transformation of the potential which keeps its shape and depth unchanged but shifts the minimum to a different value $\beta_{\min}^{\text{new}}$ can be achieved by multiplying the potential parameters (C_k , D_6) with the corresponding ratio $(\beta_{\min}/\beta_{\min}^{\text{new}})^k$. Appreciable but still smooth changes in the potential shape are associated with deviations from the general tendency of absolute increase of the parameters with decreasing deformation in the heavier isotopes. As already mentioned, the real motion of the β and γ degrees of freedom is realized in a potential which is mathematically constructed from the contributions of six different terms. Although the roles of these terms can be associated with physical effects, they do not have the meaning of separate independent potentials (interactions) and reveal themselves only when summed up in $V(\beta, \gamma)$. For example, one could imagine a case of a PES parametrizable in a nonunique way by a sufficiently complicated function of β and γ which contains many parameters. The calculated nuclear properties would be not influenced at all if two different parametrizations of the same physical PES are used.

The calculated level schemes are compared to the experimental ones in Fig. 3 and Table II. Before addressing these results (as well as the description of the electromagnetic properties) in Sec. III, however, it may be

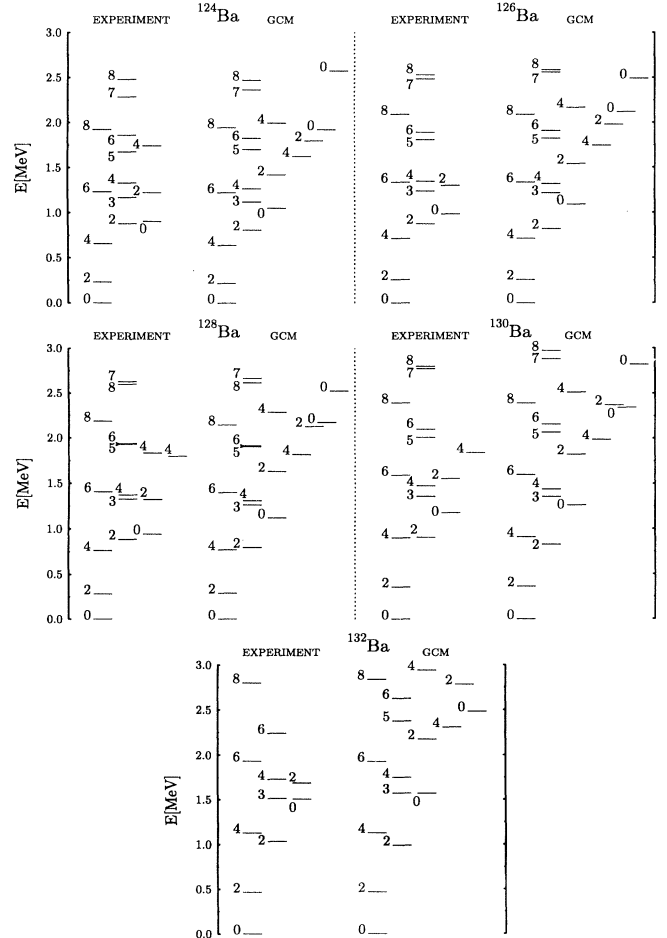


FIG. 3. Calculated and experimental level schemes of $^{124-132}\text{Ba}$.

worth discussing for the interested reader some “technical” aspects of the fitting procedure. They are related to the uniqueness of the results derived and the ambiguities which may arise in a case where no sufficient data are available as it is in ^{132}Ba .

Uniqueness of the derived potentials $V(\beta, \gamma)$. The PES's in the present work were obtained by an optimizing fit where both overall agreement with the experimental data and the description of some special features have been paid attention. Therefore, we do not claim that our final potential and kinetic energy parameters are unique nor there are not other classes of potentials which could (at least partly) describe the data. The smooth evolution (Fig. 2) and the qualitative agreement (cf. Sec. III B) of the PES derived with the results of microscopic nuclear shape calculations suggest, however, that the basic trends

TABLE II. Calculated (th) and experimental (expt) level energies in MeV. For 0_1^+ levels, the absolute theoretical ground-state energy is also shown (in brackets). The theoretical 4_4^+ state is assigned to the 0_2^+ band. See caption to Fig. 1 for experimental references.

Level		^{124}Ba	^{126}Ba	^{128}Ba	^{130}Ba	^{132}Ba
0_1^+	th	0[-3.463]	0[-3.044]	0[-2.742]	0[-2.557]	0[-1.646]
	expt	0	0	0	0	0
2_1^+	th	0.217	0.257	0.291	0.363	0.467
	expt	0.230	0.256	0.284	0.357	0.465
4_1^+	th	0.634	0.714	0.771	0.912	1.128
	expt	0.651	0.711	0.763	0.901	1.128
6_1^+	th	1.218	1.335	1.400	1.599	1.928
	expt	1.228	1.333	1.407	1.593	1.933
8_1^+	th	1.943	2.090	2.149	2.393	2.840
	expt	1.922	2.090	2.189	2.395	2.801
2_2^+	th	0.804	0.819	0.797	0.827	0.990
	expt	0.872	0.874	0.885	0.907	1.032
3_1^+	th	1.116	1.214	1.266	1.355	1.571
	expt	1.162	1.236	1.326	1.360	1.511
4_2^+	th	1.262	1.315	1.312	1.437	1.750
	expt	1.324	1.345	1.372	1.477	1.729
5_1^+	th	1.670	1.823	1.910	2.006	2.377
	expt	1.672	1.808	1.931	2.012	
6_2^+	th	1.825	1.907	1.920	2.156	2.626
	expt	1.857	1.890	1.939	2.101	2.241
7_1^+	th	2.362	2.559	2.665	2.880	3.281
	expt	2.284	2.485	2.631	2.774	
8_2^+	th	2.470	2.585	2.616	2.972	3.592
	expt	2.478	2.530	2.601	2.799	
0_2^+	th	1.045	1.089	1.120	1.262	1.569
	expt	0.898	0.984	0.943	1.179	1.504
2_3^+	th	1.415	1.539	1.634	1.823	2.176
	expt	1.217	1.297	1.322	1.557	1.686
2_4^+	th	1.796	1.980	2.132	2.370	2.784
	expt					
4_3^+	th	1.621	1.744	1.823	1.987	2.310
	expt			1.801	1.844	
4_4^+	th	1.992	2.167	2.288	2.511	2.943
	expt	1.739		1.835		
0_3^+	th	1.920	2.118	2.176	2.342	2.485
	expt					
0_4^+	th	2.574	2.489	2.526	2.818	3.392
	expt					

of the shape evolution are correctly reproduced. On the other hand, the results of the fitting procedure strongly depend on the amount, quality, and sensitivity of the data involved. The experimental quadrupole moments are of special importance because all other observables [level energies and $B(E2)$'s] are virtually not influenced under reflection of the Hamiltonian with respect to the $\gamma = 30^\circ$ axis. An other problem is the correct identification of the collective states whose characteristics can be included as input data in the fitting procedure. We found this problem at $A \geq 132$ and it has prevented us from pursuing the systematics towards heavier isotopes.

The difficulties in ^{132}Ba arise due to the lack of complete experimental data on the γ band and the cascade based on the 0_2^+ level (Fig. 3). In particular, the last known level of the γ band is the 4_2^+ one and an assignment of the 6_2^+ level to this band is questionable (the energy of the $6_2^+ \rightarrow 4_2^+$ transition is only 73% of that of the $4_2^+ \rightarrow 2_2^+$ one [26] what is not observed in the lighter isotopes). Further, the assumption that the 2_3^+ level is the second member of the 0_2^+ band is not fully consistent with the relative strengths of the depopulating transitions. The transition $2_3^+ \rightarrow 2_1^+$ is characterized by an unexpectedly large $B(E2)$ branching ratio [25] whereas the $0_2^+ \rightarrow 2_1^+$ transition (from the bandhead) is not observed. This could be, however, due to a strong unresolved $M1$ admixture. The much larger apparent moment of inertia of the 0_2^+ band in comparison to the g.s.b. (if the experimental 2_3^+ level is indeed a band member) also indicates complications challenging the model description. In addition, the 2_2^+ level is connected to the 2_1^+ one by the strongest transition within the $B(E2, 2_2^+ \rightarrow 2_1^+)$ systematics of stable even-even nuclei with $40 \leq A \leq 190$ which may point at the existence of experimental problems. In the fitting procedure, depending on what data are given more weight, several potentials were found which provide fragmentary descriptions of the data. Although the results for ^{132}Ba are quite ambiguous, we include in the systematics one of these potentials [Fig. 2(b)] in order to give some hints on possible trends of the shape evolution in the heavier barium isotopes.

III. RESULTS

In this section, the spectroscopic properties obtained in the framework of the GCM (calculated level schemes and electromagnetic transition probabilities) are first compared to the experimental data in order to estimate the goodness of the fits and provide a basis for the following discussion. Then we proceed with a presentation of the main features of the PES derived and compare them to the results of nuclear shape calculations based on different approaches.

A. Description of spectroscopic properties

1. Level energies

In general, as it can be seen from Fig. 3 and Table II the energies of the levels of the ground-state and γ

bands are reproduced very well. The existence of these collective band structures is indeed supported by the calculated strong intraband $E2$ transitions (cf. Table III and discussion in Sec. III A 2). We note only the somewhat lower energy of the theoretical 2_2^+ state as well as the tendency of the staggering at higher spin in ^{130}Ba which is not completely described. The energy position of the 4_3^+ state (experimentally associated in $^{128-130}\text{Ba}$ with a double γ excitation) is also reasonably well reproduced. The most serious problems in reproducing the energy spectra are associated with the bandhead position and the level spacing of the excitations based on the 0_2^+ levels. The character of these excitations will be discussed in more detail in Sec. IV A. Here we mention only its relation with the structure of the potential in the γ direction (and especially in $^{124-128}\text{Ba}$, with the shallow oblate minimum appearing in the PES) as well as with the deformation dependence of the mass parameters. No other effects were found which would be able to lower the energy of this state without a deterioration of the description of the ground-state and γ bands which were already well reproduced by the presented fits. A larger discrepancy (compared to the bandhead position) is the small calculated moment of inertia of the band based on the 0_2^+ level. A deeper oblate minimum may be expected

to correct for this drawback but then the effects of γ softness (like the staggering) would be affected. Therefore, we prefer to attribute less weight to the results for the 0_2^+ band unless more sensitive experimental data as, e.g., absolute $B(E2)$ transition strengths and quadrupole moments are available.

2. Quadrupole properties

Absolute $E2$ transition strengths. Some of the calculated absolute $B(E2)$ values (as a rule, those of the strongest transitions depopulating a given initial level) are compared to the experimental ones in Table III. In most of the cases, the $B(E2)$ strengths are in agreement with the experimental data within the statistical limits of 1–2 σ (standard deviations). Three exceptions, however, have to be mentioned. Two of them may be related to experimental problems. These are the transitions $2_2^+ \rightarrow 2_1^+$ in ^{132}Ba and $8_1^+ \rightarrow 6_1^+$ in ^{126}Ba . As already mentioned (Sec. II B), in ^{132}Ba the experimental value [25] of $B(E2, 2_2^+ \rightarrow 2_1^+) = 0.587(96) e^2 b^2$ is certainly too large. Concerning the $8_1^+ \rightarrow 6_1^+$ transition in ^{126}Ba , its measured [30] $B(E2)$ strength is the smallest one in the g.s.b. of that nucleus and probably indicates exper-

TABLE III. Some calculated (*t*) and experimental (*e*) $B(E2)$ reduced transition probabilities (in units of $e^2 b^2$) in $^{124-132}\text{Ba}$. The theoretical values are obtained with the full $E2$ operator from Eq. (5) including terms quadratic in $\alpha_{2\mu}$. Experimental data are taken from ^{124}Ba [29], ^{126}Ba [30], ^{128}Ba [31,32], ^{130}Ba [33,34], and ^{132}Ba [25].

$I_i^+ \rightarrow I_f^+$		124	126	128	130	132
$0_2 \rightarrow 2_2$	th	0.265	0.295	0.337	0.258	0.178
$0_3 \rightarrow 2_1$	th	0.015	0.034	0.082	0.087	0.097
$0_4 \rightarrow 2_4$	th	0.081	0.197	0.489	0.435	0.301
$2_1 \rightarrow 0_1$	th	0.405	0.312	0.276	0.203	0.174
	expt	0.398(16)	0.304(32) ^a	0.293(16) ^b	$\leq 0.203^a$	0.172(16)
$2_2 \rightarrow 2_1$	th	0.066	0.095	0.152	0.211	0.229
	expt			0.132(52)	0.278(38)	0.587(96)
$2_3 \rightarrow 0_2$	th	0.234	0.188	0.175	0.158	0.167
$2_4 \rightarrow 2_3$	th	0.473	0.404	0.381	0.327	0.291
$3_1 \rightarrow 2_2$	th	0.583	0.424	0.364	0.295	0.288
$4_1 \rightarrow 2_1$	th	0.609	0.476	0.420	0.302	0.263
	expt	0.626(15)	0.436(37)	0.437(36)		
$4_2 \rightarrow 2_2$	th	0.266	0.218	0.207	0.161	0.139
	expt			0.396(117) ^b		
$4_3 \rightarrow 4_2$	th	0.215	0.215	0.222	0.210	0.223
$4_4 \rightarrow 2_3$	th	0.257	0.237	0.242	0.230	0.243
$5_1 \rightarrow 3_1$	th	0.408	0.320	0.284	0.212	0.189
$6_1 \rightarrow 4_1$	th	0.709	0.561	0.495	0.358	0.322
	expt	0.637(24)	0.491(218)	0.565(130)		
$6_2 \rightarrow 4_2$	th	0.438	0.344	0.317	0.245	0.208
	expt			0.529(84)		
$7_1 \rightarrow 5_1$	th	0.590	0.464	0.409	0.303	0.271
$8_1 \rightarrow 6_1$	th	0.780	0.618	0.541	0.396	0.367
	expt	0.643(74)	0.298(108)	0.465(155)		
$8_2 \rightarrow 6_2$	th	0.467	0.393	0.378	0.302	0.253
	expt			0.466(117)		

^aValues reduced in order to take into account the nuclear deorientation effect whose underestimation leads to the determination of shorter lifetimes in the specific case (see Refs. [28,33]).

^bIn a coincidence RDDS measurement [32], the values $B(E2, 2_1^+ \rightarrow 0_1^+) = 0.276_{-0.170}^{+0.094}$ and $B(E2, 4_2^+ \rightarrow 2_2^+) = 0.218_{-0.055}^{+0.109}$ are determined.

imental problems in the lifetime determination. Such problems may be related, e.g., to the correct accounting for the feeding from higher-lying states. More problematic is the situation with the $6_2^+ \rightarrow 4_2^+$ transition in ^{128}Ba . In the γ band of that nucleus, the fast increase of the $B(E2, I \rightarrow I - 2)$ values with increasing spin I has been already noticed in Ref. [31]. This feature is reproduced to some extent (quantitatively at the 8_2^+ level) by the present calculations but a deviation from the data still remains. It is interesting to note that in the case of a nearly γ -independent potential the calculated $B(E2)$ values in the γ band come closer to the data. However, since other important features and especially the simultaneous description of the level energies in the g.s.b. and γ band are affected in the wrong direction we prefer the potential presented in Fig. 2(a) which is more structured with respect to the γ degree of freedom.

Quadrupole moments. The calculated quadrupole moments are presented in Table IV. Experimentally, the only known quadrupole moment is that of the 2_1^+ state in ^{130}Ba : $Q_{\text{expt}}(2_1^+) = -1.02 \pm 0.15$. The theoretical value $Q(2_1^+) = -0.535$ has the right sign but is about a factor of 2 smaller. In our opinion, this degree of agreement can be considered as satisfactory. The calculated quadrupole moments are closely related to the shape characteristics of the excited states. Thus, the relatively large quadrupole moments (e.g., $|Q| \geq 0.7$ e b) in the beginning of the isotopic chain decrease (absolutely) with increasing mass number A . This effect points to a relocation of the wave functions towards the $\gamma = 30^\circ$ axis which leads in some cases to a change of the sign of the quadrupole moment Q .

$B(E2)$ branching ratios. Some of the calculated branching ratios are presented in Fig. 4 together with the results of calculations in the framework of other collective models (cf. Sec. IV A). An overall qualitative agreement is observed in reproducing the main features of the data. The strongest transitions (with a branching $\geq 20\%$) are well reproduced and only in few cases deviations within a factor of 2 are observed. We recall also the overall good

TABLE IV. Quadrupole moments (in e b) of the low-lying states in $^{124-132}\text{Ba}$ obtained with the full $E2$ operator from Eq. (5). The only known experimental value [34] is that for the 2_1^+ level in ^{130}Ba $Q(2_1^+) = -1.02(15)$.

I_i^+	124	126	128	130	132
2_1	-1.240	-1.040	-0.876	-0.535	-0.372
2_2	1.127	0.924	0.770	0.479	0.348
2_3	0.218	0.197	0.189	-0.007	-0.270
2_4	-0.330	-0.251	-0.205	-0.004	0.264
4_1	-1.556	-1.290	-1.047	-0.565	-0.376
4_2	-0.056	0.180	0.294	0.205	0.232
4_3	0.843	0.531	0.338	0.209	0.135
4_4	0.678	0.468	0.396	0.093	-0.250
5_1	0.810	0.600	0.400	0.117	-0.022
6_1	-1.681	-1.366	-1.042	-0.470	-0.311
6_2	-0.160	0.099	0.195	0.110	0.261
7_1	1.111	0.815	0.507	0.085	-0.114
8_1	-1.718	-1.349	-0.917	-0.320	-0.228
8_2	0.251	0.266	0.191	0.088	0.370

agreement between the calculated and experimental absolute $B(E2)$ values in Table III. The quantitative description of weak transitions is, however, less satisfactory. In model calculations, such transitions appear in a natural way between small components of the initial and final state wave functions and/or due to cancellation in the matrix elements. Since the present GCM wave functions are expressed in a basis where a large number of components have appreciable contributions (cf. Sec. IV B) the cancellation effects may be expected to play an important role. Although the calculated $B(E2)$ branching ratios reproduce some rather small experimental quantities within the error bars (Fig. 4) differences within an order of magnitude exist in other cases. The discrepancy is even larger (orders of magnitude) in the cases of the $2_2^+ \rightarrow 0_1^+$ and $3_1^+ \rightarrow 2_1^+$ transitions in $^{124-128}\text{Ba}$. It was found that the reason for such small values is a double cancellation in the matrix elements. The first term $Q_2^{(1)}$ in the $E2$ operator [Eq. (5)] gives rise to destructively interfering partial contributions while the total contribution from the second term $Q_2^{(2)}$ turns out to be of the opposite sign and in the extreme cases in ^{128}Ba , of approximately the same magnitude. It should be noticed that an improvement of the description of the $B(E2, 2_2^+ \rightarrow 0_1^+)/B(E2, 2_2^+ \rightarrow 2_1^+)$ branching ratio in ^{128}Ba is easily obtained with a nearly γ -independent potential. However, as in the case of the $E2$ transitions in the γ band of the same nucleus (cf. above) the improvement of this particular aspect of the data description significantly worsens the quantitative agreement obtained for the level energies and some absolute $E2$ transition strengths as for instance the $B(E2, 2_2^+ \rightarrow 2_1^+)$ one. A discrepancy concerning the same branching ratio in the framework of the GCM was already discussed [13] for the case of some γ soft osmium isotopes. The authors suggested that the assumptions leading to the present form of the GCM quadrupole operator [Eq. (5)] are too crude, especially the lack of distinction between neutrons and protons. Since further theoretical efforts are required to solve this problem, we performed only some checks of the role of the different terms in the operator. First, we tried to take into account the third-order terms ($\sim \beta^3$). Using the corresponding expression for the modified $E2$ operator [cf. Eq. (57) in Chap. 3 and Eq. (162a) in Chap. 8 of Ref. [36]] we recalculated the matrix elements. No improvement occurred in the branching ratios at the 2_2^+ and 3_1^+ levels because the contribution from the new terms was only of few percent. Thus, the reasons for the calculated very weak $E2$ transition strengths $2_2^+ \rightarrow 0_1^+$ and $3_1^+ \rightarrow 2_1^+$ are more likely not due to missing higher-order terms in the $E2$ operator. In a second attempt, the calculation of the electromagnetic quantities were performed using only the first term $Q_2^{(1)}$. Here, a value $R_0=1.2$ fm $A^{1/3}$ was employed in order to reproduce again the $B(E2, 2_1^+ \rightarrow 0_1^+)$ transition strengths. In general, the description of the strong transitions (e.g., those in Table III) does not deteriorate compared to the results obtained with the two terms ($Q_2^{(1)} + Q_2^{(2)}$). This can also be seen in Fig. 4 by comparing the correspondingly labeled GCM calculations. An improvement is observed for the calculated small branching ratios of the $2_2^+ \rightarrow 0_1^+$ and $3_1^+ \rightarrow 2_1^+$

transitions in $^{124-128}\text{Ba}$ although it is not sufficient to reproduce the experimental data. However, the description of the same quantities in $^{130-132}\text{Ba}$ becomes worse. In our opinion, the above checks suggest that better results may be obtained by using an effective $E2$ operator where the contributions of the two terms should be not strictly fixed by the purely geometrical factor $-\frac{10}{\sqrt{70\pi}}$ as it is in Eq. (5).

B. Shape evolution

In the framework of the GCM, the notion of nuclear shape has several aspects. Thus, one could associate it with the PES and their physical parameters which facilitates the comparison with results of microscopic calculations. On the other hand, each state has its own probability distribution in the β - γ plane whose moments $\langle\beta\rangle$, $\langle\beta^2\rangle$, $\langle\gamma\rangle$, etc. may differ from state to state. This makes

the effect of shape coexistence an inherent property of the GCM. In this context, we first discuss in the present section both potentials and mean shape parameters of the excited states as derived by the fitting procedure. Further, these quantities are compared to the results of microscopic nuclear shape calculations.

1. GCM results

Potentials. The shape evolution presented by the potentials in Fig. 2 reveals the following features.

(i) The global minimum of the potential is always at $\gamma = 0^\circ$ (prolate) and a gradual decrease of β_{\min} is observed when the mass number A increases towards the $N = 82$ neutron shell closure. This change of the deformation is accompanied by a decrease of the potential depth. It should be mentioned that the minimal values of $V(\beta, \gamma)$ at fixed angles $\gamma > 0$ lie at somewhat smaller deformation β than the prolate minimum (cf., e.g., the potential

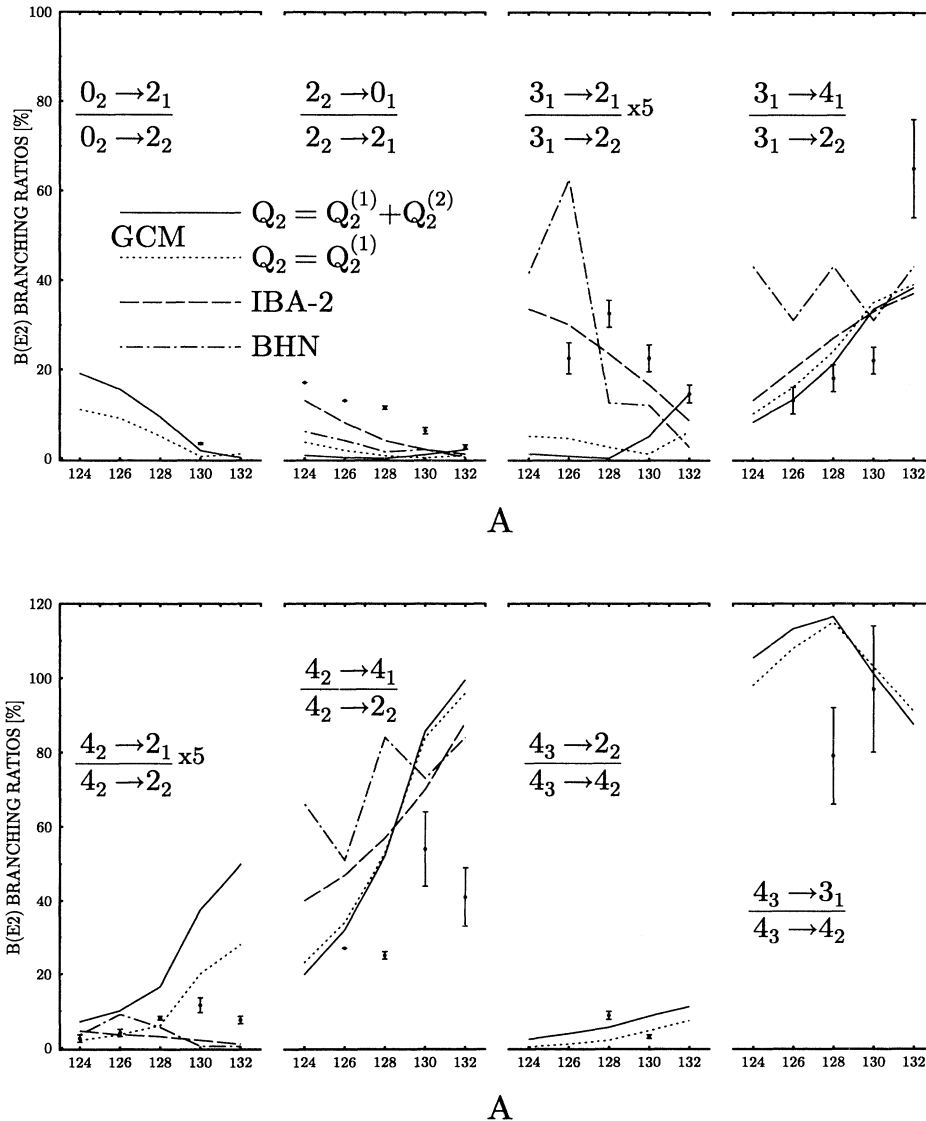


FIG. 4. Some calculated and experimental $B(E2)$ ratios in $^{124-132}\text{Ba}$ vs mass number A . Two variants of the GCM calculations are displayed with $(Q_{2\mu}^{(1)} + Q_{2\mu}^{(2)})$ and without $(Q_{2\mu}^{(1)})$ the second term in the quadrupole operator [Eq. (5)]. Results of the calculations of Puddu *et al.* [35] (IBA-2) and Rohozinski *et al.* [8] (BHN) are also presented. See also text.

projections at $\gamma = 0^\circ$ compared to those at $\gamma = 30^\circ$ and 60° in Fig. 2).

(ii) A shallow secondary oblate ($\gamma = 60^\circ$) minimum is present in ^{124}Ba which virtually disappears in $^{126-128}\text{Ba}$.

(iii) A prolate-oblate energy difference $V_{\text{PO}}^{0^\circ-60^\circ}$ of the order of 30% of the potential depth exists in $^{124-130}\text{Ba}$ ($V_{\text{PO}}^{0^\circ-60^\circ} = \min[V(\beta, 60^\circ)] - \min[V(\beta, 0^\circ)]$, cf. also Table I). The stiffness in the γ direction around the prolate minimum decreases with increasing mass number A . However, even in the lighter isotopes the contour of the absolute energy of the ground state (the thicker lines on the r.h.s. of Fig. 2) covers the entire sector $\gamma = 0^\circ-60^\circ$.

(iv) A specific feature of the potentials derived are the γ profiles $V(\beta = \text{const}, \gamma)$ for β values in the vicinity of β_{min} ($\beta \leq \beta_{\text{min}}$). They are illustrated in Fig. 5. In $^{124-128}\text{Ba}$, a well-pronounced minimum on the prolate side coexists with a more or less flat γ dependence at, e.g., $\gamma > 20^\circ$. This effect is especially pronounced in ^{128}Ba due to the (virtual) disappearance of the shallow oblate minimum. In ^{128}Ba , $V(\beta_{\text{min}}, 30^\circ) \approx V(\beta_{\text{min}}, 60^\circ)$ whereas in $^{124-126}\text{Ba}$ the projections $V(\beta, 30^\circ)$ and $V(\beta, 60^\circ)$ cross each other at deformations $\beta < \beta_{\text{min}}$. Thus, the potential structure around $\gamma = 30^\circ$ (Fig. 2) which acts as a kind of potential barrier between prolate and oblate shapes in the lighter isotopes disappears in ^{128}Ba .

(v) Throughout the isotopic chain, the stiffness in the β direction is always larger than that in γ , i.e., these nuclei are characterized by an appreciable γ softness.

Mean shape characteristics. A different look at the shape evolution in the isotopic chain is given by the mean values and the widths of the distributions of the shape variables β and γ . The corresponding quantities characterizing the bandheads of the g.s. and γ bands are presented in Table V. The considerable width σ_γ of the distributions in the γ direction illustrates again the γ softness of the nuclei. We note the difference in $\langle \gamma \rangle$ for the 0_1^+ and 2_2^+ states which could be an explanation of the difficulties faced by the simultaneous description of the energies of the g.s. and γ bands by using a nearly γ -independent potential (Sec. II B). The effect decreases

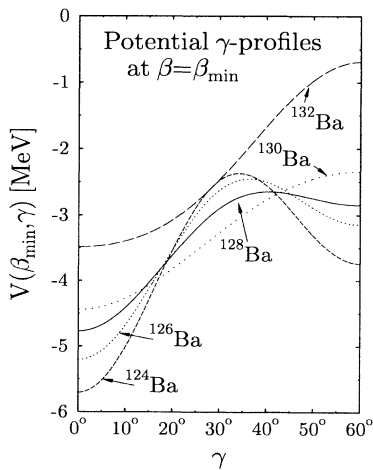


FIG. 5. γ dependence of the potentials derived for $^{124-132}\text{Ba}$ at the potential minimum ($\beta = \beta_{\text{min}}$).

TABLE V. Derived mean shape parameters for the 0_1^+ and 2_2^+ states in the investigated Ba isotopes. See also text.

A	β_{rms}		σ_β		$\langle \gamma \rangle$		σ_γ	
	0_1^+	2_2^+	0_1^+	2_2^+	0_1^+	2_2^+	0_1^+	2_2^+
124	0.299	0.295	0.056	0.054	8.5°	16.0°	15.6°	13.2°
126	0.264	0.262	0.053	0.049	10.9°	18.9°	14.5°	12.9°
128	0.248	0.251	0.050	0.046	14.1°	21.6°	13.3°	11.8°
130	0.215	0.225	0.045	0.041	17.0°	21.2°	12.5°	11.7°
132	0.200	0.216	0.045	0.041	17.6°	19.9°	12.1°	11.2°

with increasing mass number A and has to be associated with the more complicated γ dependence of the potentials of the lighter isotopes (cf., e.g., Fig. 5). At the same time, the $\langle \gamma \rangle$ values characterizing the 2_2^+ state display a rather constant behavior (with a tendency of small increase towards the heavier isotopes). This feature is consistent with the empirical conclusion (suggested by the systematics of the level energies in Fig. 1) that the excitation of the γ degree of freedom is a property which is exhibited in a remarkably similar way by all investigated nuclei. In ^{130}Ba , the ground-state GCM shape parameters $\beta_{\text{rms}}(0_1^+) = 0.215$ and $\langle \gamma(0_1^+) \rangle = 17^\circ$ can be compared with those derived according to the recently developed approximation [37] of the sum-rule method, namely $\beta_{\text{rms}} = 0.23$ (1) and $\langle \gamma \rangle = 20^\circ$ (3°). Both parameters are in reasonable agreement.

Deformation-dependent mass parameters. An important complement to the picture presented by the PES is the significant deformation (γ and/or β) dependence of the mass parameters and inertial functions of the collective Hamiltonian which is revealed by the relatively high values of the parameter P_3 (Table I). This dependence was already deduced by Rohozinski *et al.* [8] for the nuclei of the $A = 130$ mass region on the basis of microscopic calculations. Although the anharmonicity (P_3) term of the GCM Hamiltonian may be in some cases only a rough simulation of the above dependence, the sensitivity of the model to such effects can be considered as an advantage. The anharmonicity term could favor a localization of the wave function in a particular region of the β - γ plane. Therefore the real shape of the nucleus can be best represented by a probability distribution in this plane as illustrated for the case of the 0_1^+ and 0_2^+ states in Sec. IV A.

2. Comparison with microscopically calculated PES

Before addressing the results obtained in the framework of different theoretical approaches it is worth discussing up to what limits these data are really comparable. For instance, a group of macroscopic-microscopic approaches to derive the potential $V(\beta, \gamma)$ is based on: (i) calculation of the deformation energy of the nucleus considered as a liquid drop and (ii) correction for shell effects by means of the Strutinsky method [38]. Such calculations could differ, e.g., with respect to the employed deformed *single-particle* potentials. Thus, we shall consider below the extensive calculations by Ragnarsson *et al.* [39] based on the modified harmonic oscillator (MHO) poten-

tial as well as the calculations by Kern *et al.* [40] where a Woods-Saxon (WS) potential was used. It seems natural to associate the potentials $V(\beta, \gamma)$ obtained thereby with the deformation energy of the ground state of the nucleon system at different quadrupole deformations. In a next step, the mass parameters and inertial functions appearing in the Bohr Hamiltonian (denoted by BH in the present section) can be calculated and the eigenvalue problem solved as done, e.g., in Ref. [8]. Since dynamics effects are taken into account only at this stage, it is clear that the energy of the zero-point vibrations cannot be precisely obtained in this way. Therefore the absolute depth of the BH (and of the GCM) potential must not necessarily coincide with the results of the macroscopic-microscopic calculations. On the other hand, the GCM potentials are derived by fitting the properties of the low-lying collective states. Hence they could reproduce the BH potential provided that the functional dependence on the quadrupole variables in Eqs. (2) and (3) is a good approximation for the particular case. However, even in such a favorable situation the fitted experimental data could reflect the presence of other, not always both collective and quadrupole degrees of freedom as, e.g., the hexadecapole deformation or the polarization of the core by specific quasiparticle orbitals. The former was shown [9] to be important for the description of the equilibrium deformation in ^{128}Ba . A somewhat more technical aspect of the problems faced by the comparison is the correspondence between characteristic values of the deformation parameter β , e.g., the position of the potential minimum β_{\min} . (We do not consider here possible differences due to the parametrization of the deformation of the nuclear ellipsoid or to effects of not completely overlapping mass and charge distributions.) Thus, the values β_{\min} obtained in the present work (Table I) depend on the factor $R_0 = r_0 A^{1/3}$ fm which accounts (at the power

of two) for the dependence of the collective $E2$ operator on the nuclear radius. Since β_{\min} is (mainly) determined by the reproduction of the $B(E2, 2_1^+ \rightarrow 0_1^+)$ transition strength one can expect some deviation towards higher values in our results which are obtained with $r_0=1.15$ (see also Sec. II A). Using $r_0=1.2$ would reduce the β_{\min} values by roughly 8%. Taking into account the above considerations, an exact coincidence between the PES derived by the GCM fits and the ones calculated within macroscopic-microscopic approaches could hardly be expected and an agreement should be searched basically on a qualitative level.

In Table VI, some global characteristics of the potentials derived in the present work are compared to the corresponding quantities obtained in previous theoretical calculations. These are the position β_{\min} of the PES minimum and prolate-oblate energy difference $V_{\text{PO}}^{0^\circ-60^\circ}$. The quantity $\beta_{\text{rms}}(0_1^+)$ characterizing the ground-state quadrupole deformation (which includes dynamic effects) is also shown. Apart from the already mentioned MHO and WS calculations, data are taken from the numerical solution [8] of the Bohr Hamiltonian (labeled by BHN) and the self-consistent mean-field calculations [41] of triaxial deformation energy surfaces based on a constraint Hartree-Fock+BCS approach (labeled by HF+BCS). In addition, the equilibrium deformation parameters deduced by Möller *et al.* [42] in assuming axially symmetric shapes are displayed (labeled by M).

In general, a prolate absolute minimum is favored in the investigated nuclei except for the MHO calculations which predict an oblate equilibrium deformation in ^{126}Ba and the BHN calculations which predict oblate minima in $^{124-126}\text{Ba}$ whereas in the heavier isotopes the minima are shifted to $34^\circ-20^\circ$. The positions of the PES minima β_{\min} seem to be overestimated by the GCM but differ-

TABLE VI. Comparison of the position β_{\min} of the absolute minimum of the PES in β and the prolate-oblate energy difference $V_{\text{PO}}^{0^\circ-60^\circ} = \min[V(\beta, 60^\circ)] - \min[V(\beta, 0^\circ)]$ (in MeV) as derived in the present work (GCM) and nuclear shape calculations based on different approaches (cf. text). In all cases, the minimum is lying on the prolate side ($\gamma = 0^\circ$) with the exceptions of Ref. [8] for all nuclei considered and Ref. [39] for ^{126}Ba (cf. text). The root mean squared deformation β_{rms} of the ground state is also displayed, when available.

Nucleus	GCM	WS	MHO	BHN	HF+BCS	M
		Ref. [40]	Ref. [39]	Ref. [8]	Ref. [41]	Ref. [42]
^{124}Ba	β_{\min}	0.32	0.24	0.24	0.23	0.27
	$\beta_{\text{rms}}(0_1^+)$	0.30			0.27	
	$V_{\text{PO}}^{0^\circ-60^\circ}$	1.7	1.1	0.0	-0.24	
^{126}Ba	β_{\min}	0.29	0.22	0.22	0.23	0.26
	$\beta_{\text{rms}}(0_1^+)$	0.26			0.26	
	$V_{\text{PO}}^{0^\circ-60^\circ}$	1.8	0.8	-0.1	-0.6	
^{128}Ba	β_{\min}	0.27	0.20	0.16	0.24	0.22
	$\beta_{\text{rms}}(0_1^+)$	0.25			0.24	
	$V_{\text{PO}}^{0^\circ-60^\circ}$	1.6	0.6	0.0	0.7	0.7
^{130}Ba	β_{\min}	0.23	0.17	0.15	0.20	0.17
	$\beta_{\text{rms}}(0_1^+)$	0.22			0.21	
	$V_{\text{PO}}^{0^\circ-60^\circ}$	1.6	0.5	0.1	0.6	
^{132}Ba	β_{\min}	0.21	0.14	≈ 0.12	0.17	0.14
	$\beta_{\text{rms}}(0_1^+)$	0.20			0.18	
	$V_{\text{PO}}^{0^\circ-60^\circ}$	1.7	0.3	≈ 0.05	0.2	

ences of $\Delta\beta \leq 0.06$ may be acceptable for a qualitative agreement (cf. also discussion above).

All microscopic calculations considered predict potentials with significant softness in the γ direction. It is enhanced compared to the GCM potentials in the sector $\gamma=0^\circ-30^\circ$ but the differences at $\gamma=30^\circ-60^\circ$ are minor. Concerning the prolate-oblate (PO) energy differences $V_{\text{PO}}^{0^\circ-60^\circ}$, several trends exist in the calculations discussed. On the one hand, the MHO calculations predict quite small $V_{\text{PO}}^{0^\circ-60^\circ}$ values (maximum 100 keV) in $^{124-132}\text{Ba}$. The BHN calculations use the same single-particle potential as MHO but reduced pairing effects. They predict some increase of $|V_{\text{PO}}^{0^\circ-60^\circ}|$ but due to the relative enhancement of the shell effects its dependence on the mass number A is not smooth. The WS calculations are close to the BHN results in $^{128-132}\text{Ba}$. In the lighter isotopes, however, the PO energy difference still increases when A decreases. The GCM results point at a nearly constant behavior of the $V_{\text{PO}}^{0^\circ-60^\circ}$ values which are also larger (e.g., by roughly 1.0 MeV compared to WS calculations). Thereby, the evolution of the potentials is mainly associated with the changes of the deformation (expressed by β_{min} and β_{rms}) and the γ profiles $V(\beta = \text{const}, \gamma)$.

A qualitative comparison with the results of calculations of total energy surfaces is also possible. We mention here only the calculations [43] of total Routhian surfaces (TSR) whereby the equilibrium deformation parameters obtained are close to those from Refs. [39,40]. It is interesting to note that in the TSR calculations a weak tendency for the formation of a secondary oblate minimum exists which is expressed by a saddle point appearing at $\gamma = 60^\circ$ at about the same deformation β as the main prolate minimum. However, the kinetic and potential contributions to the total energy are not resolved and therefore a quantitative comparison with the GCM results cannot be made. A similar problem arises if one considers the IBA energy surfaces [44]. Although the latter are not obtained in a microscopic way indeed, we mention them in relation with the forthcoming discussion in Sec. IV where relationships between the IBA and GCM wave functions are investigated.

Finally, the potential derived by Komatsubara *et al.* for the case of ^{124}Ba in the framework of a normal-ordered linked-cluster boson expansion theory (Fig. 11 in Ref. [45]) can be compared with the PES derived in the GCM. It has the same qualitative structure (deeper prolate minimum and a smaller oblate one) but the PO energy difference is of about 600 keV and the minima are situated at $\beta \approx 0.22$.

In the nuclei investigated, all calculations considered indicate that in the vicinity of the absolute minimum the stiffness in the β direction is larger than that in the γ direction. On the other hand, near the minima the contours of equal energy in Ref. [43] are systematically more symmetric in β compared to the GCM results. The same holds for the HF+BCS calculations in ^{128}Ba . This feature of the PES obtained within the GCM may be related to the use of polynomials in β for the expansion of $V(\beta, \gamma)$.

In our opinion, the present phenomenologically de-

rived PES are in qualitative agreement with the previous theoretical calculations considered. The new features are mainly due to the specific shape of the γ profiles $V(\beta = \text{const}, \gamma)$. As already discussed, there is a little hope to reproduce within the GCM fitting procedure all the details of microscopically calculated potentials. The comparison with the nuclear observables should decide on the reliability of the PES (Fig. 2) with respect to the main trends of the shape evolution. In this sense, the results obtained in the framework of the GCM could indicate features of the potentials which are necessary for the explanation of the data and correspondingly stimulate further refinement of the microscopic calculations.

Comparison with the BHN mean shape parameters. The calculations by Rohozinski *et al.* [8] (BHN) offer the possibility to compare shape characteristics of individual states. The values of β_{rms} agree with GCM results within $\Delta\beta = 0.02-0.03$ which is indeed closer than the differences in the positions β_{min} of the PES minima (cf. above). This effect should be due to the dynamics. The mean $\langle\gamma\rangle$ values are, however, typically closer to 30° than the GCM ones. It is interesting to note that in $^{124-126}\text{Ba}$ the mean $\langle\gamma\rangle$ values characterizing the 0_1^+ and 2_2^+ states differ by $7^\circ-9^\circ$ as in the GCM case. The widths σ_β and σ_γ are also quite close to those obtained in the present work.

IV. DISCUSSION

In this section, the spectroscopic properties obtained within the GCM are compared to the results of calculations in the framework of other collective models. The nature of the 0_2^+ state is considered in more detail. Finally, the structure of the GCM wave functions in $^{124-132}\text{Ba}$ is discussed emphasising correspondences and relationships with the IBA-1.

A. Comparison with other collective models

Among the numerous nuclear structure calculations for nuclei of the $A \approx 130$ region, we concentrate mainly on the comparison with studies [5,8,27,35,45-47] which have a more or less systematic character since this is the aspect we would like to emphasize. The discussion is limited mainly to the registration of the facts with no attempts to analyze the cases where a divergence is observed. When necessary, the specificity of the GCM results will be elucidated on the basis of the shape evolution by evoking the features of the PES derived in the present work.

Ground-state and γ -band level energies. To our knowledge, there is no calculation published up to now which gives better overall reproduction of the g.s.b. and γ band in $^{124-130}\text{Ba}$ when compared to the present GCM results. A special interest represents the simultaneous description of both bands and the behavior of the staggering in the γ band including the extreme case of ^{128}Ba . The evolution of the staggering is a crucial question which has to be accommodated with the general (both microscopically and empirically based) expectations for strong γ

softness effects in these nuclei. Some hints on the reasons for the evolution of the staggering can be obtained from a consideration of the PES derived (although a full consideration should include also the γ dependence of the mass parameters which is however difficult to visualize). Thus, the interplay of the terms V_{PO} (responsible for the prolate-oblate energy difference) and V_{NA} (nonaxial contribution) in the potential energy [Eq. (3)] leads to the changes in the profiles in γ illustrated in Fig. 5. As already mentioned, in ^{128}Ba the result is an almost γ -independent profile in the sector $30^\circ \leq \gamma \leq 60^\circ$ at $\beta \leq \beta_{\text{min}}$. The staggering effect has here a maximum in comparison with the other isotopes considered since a large-scale motion in the γ direction from the minimum of the PES and without modifying the overall deformation β can be easier achieved. The conditions for such a motion deteriorate [cf. Fig. 2(b)] in the next isotope ^{130}Ba in spite of the continuous increase of the ratio $V_S/(V_S + V_{\text{PO}} + V_{\text{NA}})$ which measures the γ -independent contribution at $\beta = \beta_{\text{min}}$ and $\gamma = 0^\circ$ (from 43% in ^{124}Ba to about 70% in ^{130}Ba).

In this way, the characteristic behavior of the staggering in the γ band for $^{124-130}\text{Ba}$ can be explained within the GCM by the interplay of γ softness, triaxiality, and changes in the γ profile between the prolate and oblate axes including the prolate-oblate energy difference. To avoid confusion, it should be noticed that here “ γ softness” and “triaxiality” are physically associated with the γ -independent term V_S and the nonaxial term V_{NA} of the potential, respectively. An “effective triaxiality” however, can arise even without an absolute potential minimum at $\gamma \neq 0^\circ, 60^\circ$ as, e.g., due to small prolate-oblate energy difference or unhomogeneities in the valley connecting the prolate and oblate axes in a nearly γ -independent potential. Generally, the notion of γ softness may be used to indicate the extent to which different potentials favour the manifestation of the γ degree of freedom. In this sense γ softness and triaxiality do not necessarily contradict each other. These two factors were already proposed [46] in the framework of the IBA for an explanation of the staggering effect in some barium and xenon isotopes. While the energy surface corresponding to a Hamiltonian with one- and two-body terms in this model is either prolate or oblate or γ unstable, the addition of a three-body (“cubic”) term brings about a triaxial deformation. (Geometrically, the latter term can be associated with the nonaxial term in the GCM potential.) Thus, a larger splitting between levels of the γ band belonging to the same τ multiplet could be obtained in comparison with the nearly complete degeneracy in the pure $O(6)$ limit [4]. In $^{128-134}\text{Ba}$, the inclusion of the cubic term makes it possible to reproduce the position of the 3_1^+ and 4_1^+ levels but the description rapidly deteriorates at higher spin. In the framework of the IBA-2, Sevrin *et al.* [47] have exploited the existence of states corresponding to overlapping prolate (oblate) and oblate (prolate) distributions of neutron and proton bosons to investigate the influence of the triaxiality induced thereby on the behaviour of the staggering. Qualitatively, their results in $^{128-130}\text{Ba}$ (Fig. 4 in Ref. [47]) reproduce the observed data trends but quantitatively

are worse than the GCM calculations. A reasonable description of the staggering in $^{124-132}\text{Ba}$ is given also by the calculations of Komatsubara *et al.* [45] without reproducing, however, the extremely low level spacing in ^{128}Ba and the inversion of the 7_1^+ and 8_2^+ levels. In that work, the energy differences $3_1^+ - 4_2^+$, $5_1^+ - 6_2^+$, and $7_1^+ - 8_2^+$ do not change significantly from ^{124}Ba to ^{132}Ba whereas the data display a clear evolution (Fig. 1 and Table II). The relatively older calculations of Refs. [8,35] do not reproduce the level spacing of the γ band. Better results are obtained in the more recent IBA-2 calculations [48] but a quantitative agreement is reached only for isotopes heavier than ^{130}Ba . It should be mentioned, however, that the latter work is more concerned with the general problem of relating the IBA-2 model parameters to microscopic quantities than with the most optimal fitting of the data.

It is interesting to note that in all theoretical calculations considered the position of the 2_2^+ level is somewhat lowered compared to the experimental one. In Ref. [45] where a normal-ordered linked-cluster boson expansion theory was used for the calculation of the potential, the effect was attributed to the influence of the last valence protons which occupy in barium the lowest $h_{11/2}$ orbits and can be expected to affect the collective motion in the γ direction. The adjustment of the energy of this orbital led to some improvement which was however not sufficient to bring the results in agreement with the experiment. In the framework of the GCM, of course, the influence of specific quasiparticle orbitals cannot be taken into account.

The electric quadrupole properties. Detailed previous results can be found in the systematic studies [8,35] as well as in Ref. [27] for $^{130-132}\text{Ba}$, Ref. [47] for $^{128-130}\text{Ba}$, Ref. [19] for ^{124}Ba , Ref. [49] for ^{130}Ba , and Ref. [48] for ^{132}Ba . Most of the quoted works are IBA calculations except for Refs. [8,27] which are based on the geometrical model (i.e., on the collective Bohr Hamiltonian). We do not consider the absolute transition strengths $B(E2, 2_1^+ \rightarrow 0_1^+)$ since they were adjusted in the fitting procedure. The strong transitions in Table III can be compared mainly to the ones calculated in Ref. [8]. In most of the cases where experimental information exists ($E2$ transitions in the g.s.b. of $^{124-128}\text{Ba}$, the γ band in ^{128}Ba) the agreement with the GCM is better. In $^{130-132}\text{Ba}$, however, the theoretical values of both approaches are quite close. The $B(E2, 2_2^+ \rightarrow 2_1^+)$ values obtained by Puddu *et al.* [35] are also close to the GCM results in these isotopes but at smaller mass number A their decrease is slower. Concerning the quadrupole moments of the 2_1^+ level in the chain considered, the predictions of Ref. [8] are positive with magnitude in the range 0.745–0.226 for $^{124-128}\text{Ba}$, $Q(2_1^+) = -0.544$ in ^{130}Ba , and $Q(2_1^+) = 0.038$ in ^{132}Ba . The value in ^{130}Ba is quite close to the GCM result of $Q(2_1^+) = -0.535$ (Table IV) but the trend of the calculations is completely different. The calculated quadrupole moments in the framework of the GCM are characterized by a gradual (absolute) decrease from relatively large negative values in the lighter isotopes towards smaller ones at $A \geq 130$. They are in quantitative agreement with the results of the IBA-2 cal-

culations [35].

As already discussed in Sec. III A 2, the branching ratios of some weak $E2$ transitions calculated within the GCM deviate significantly from the data and indicate the necessity to improve the quadrupole operator of the model [Eq. (5)]. Intuitively, the difficulties in the case of the $B(E2, 2_2^+ \rightarrow 0_1^+)/B(E2, 2_2^+ \rightarrow 2_1^+)$ ratio can be associated with the differences between the mean shape parameters $\langle \gamma \rangle$ characterizing the 0_1^+ and 2_2^+ states (cf. Table V). When these differences become smaller in $^{130-132}\text{Ba}$, the calculated branching ratios come closer to the experimental data (Fig. 4). The comparison with other models demonstrates that they reproduce better particular branching ratios. For instance, as one can see in Fig. 4, the $B(E2, 2_2^+ \rightarrow 0_1^+)/B(E2, 2_2^+ \rightarrow 2_1^+)$ ratio is better described (within a factor of 2) by the IBA-2 calculation [35] which reproduces almost exactly another problematic ratio: the $B(E2, 3_1^+ \rightarrow 2_1^+)/B(E2, 3_1^+ \rightarrow 2_2^+)$ one. However, the description of the strong intraband transitions from the γ band (e.g., $3_1^+ \rightarrow 4_1^+$, $4_2^+ \rightarrow 4_1^+$) are of similar quality in the GCM and IBA-2. We note that for $A \geq 130$ the ratios $B(E2, 3_1^+ \rightarrow 4_1^+)/B(E2, 3_1^+ \rightarrow 2_2^+)$ and $B(E2, 4_2^+ \rightarrow 4_1^+)/B(E2, 4_2^+ \rightarrow 2_2^+)$ calculated in all theoretical approaches presented in Fig. 4 are close to the corresponding O(6) values of 40 and 91, respectively. The values obtained in Ref. [8] for the nuclei with $A \leq 128$ are enhanced compared to the experimental data. The IBA calculations [19,47–49] for single (or few) isotopes in the isotopic chain considered give in general better (or at least similar) description of the corresponding branching ratios as the GCM does.

Description of the 0_2^+ band. Most of the calculations considered (including the present ones) fail to reproduce fully satisfactory the low-lying 0_2^+ bands in $^{124-128}\text{Ba}$. The only exception is the work of Idrissi *et al.* [19] where a reasonable description of that band in ^{124}Ba is obtained in the framework of the IBA-2 despite the somewhat vibrational-like behavior exhibited by the sequence of the theoretical band levels. However, the interpretation by the authors of the 0_2^+ state as a β bandhead is not really supported by the $B(E2)$ transition strengths calculated in their work [19]. Generally, β -vibrational states are expected to decay preferentially to the g.s.b. while those calculations predict for the levels of the 0_2^+ band a stronger decay to the γ band. As noticed in Ref. [50], the low-lying 0^+ states in the $A = 130$ mass region could have a more complicated nature than the one implied by the simple geometrical interpretation in terms of β or (two-phonon) γ vibrations. Indeed, complementary experimental information is needed for clarifying the nature of these excitations. Although the GCM calculations do not describe fully satisfactory the 0_2^+ band we briefly discuss the results obtained, also with the aim to illustrate the advantages of the geometrical approach of the model with respect to the visualization.

An interpretation in terms of a two-phonon γ vibration seems unlikely due, e.g., to the energy position of the 0_2^+ state. However, an association of the band with an excitation with respect to the γ degree of freedom is supported and a β -vibrational character rejected by the following reasons: (i) The PES in Fig. 2 indicate

a relatively higher stiffness in the β direction compared to the stiffness in γ . (ii) The small branching ratios $B(E2, 0_2^+ \rightarrow 2_1^+)/B(E2, 0_2^+ \rightarrow 2_2^+)$. (iii) The comparison of the number of nodes in β of the wave functions of the ground and 0_2^+ states does not reveal the relation $\langle n_\beta(0_2^+) \rangle \approx \langle n_\beta(\text{g.s.}) \rangle + 1$ which should be expected for a β -vibrational state [cf. Eq. (8)]. States with properties close to the ones expected for a β vibration are predicted by the GCM calculations at higher energy.

These arguments are further supported by the evolution of the properties of the 0_2^+ state along the isotopic chain. The relative energy position of the 0_2^+ state displays a significant evolution which is (at least partly) related to the changes in the potential within the sector 30° – 60° and especially to the secondary oblate minimum in the PES. This is supported by the calculated positive quadrupole moments of the 2_3^+ level in $^{124-128}\text{Ba}$ (Table IV). In $^{130-132}\text{Ba}$, the 0_2^+ state can be already associated with the 0^+ state of the O(6) limit of the IBA characterized by the quantum numbers $\sigma = N$, $\tau = 3$, and $\tilde{\nu}_\Delta = 1$ (see also Ref. [18]) or with a member of the quadruplet $I = 0^+, 3^+, 4^+, 6^+$ of the model of Wilets and Jean ($\lambda = 3$, $n_\beta = 0$). In our calculations, the 0_2^+ state is characterized by a rather constant mean value $\langle \mu \rangle \approx 1.2$ (cf. next section, Fig. 8) of the number of phonon triplets coupled to angular momentum zero. In comparison, the g.s. wave functions display an evolution in $\langle \mu \rangle$ from ^{124}Ba to ^{132}Ba which points at an increasing difference between the μ structure of the wave functions of the 0_1^+ and 0_2^+ states. The increasing structural differences are reflected also by the gradual decrease of the calculated ratio $B(E2, 0_2^+ \rightarrow 2_1^+)/B(E2, 0_2^+ \rightarrow 2_2^+)$ in the heavier isotopes.

Finally, information on the physical nature of the 0_1^+ and 0_2^+ states is provided by the contour plots of the probability distributions given by the squared wave functions at different points of the β - γ plane which are presented in Fig. 6. [We note that the volume element $\propto \beta^4 \sin(3\gamma)$ is taken into account.] The evolution of the ground state can be associated mainly with a gradual decrease of the coordinate $\beta \cos(\gamma)$ of the peak of the distribution with increasing mass number A . Since the coordinate $\beta \sin(\gamma)$ virtually does not change, an increasing portion of the distribution enters the sector 30° – 60° in the heavier isotopes. The expectation value of $\beta \sin(\gamma)$ can be considered as a measure of both eccentricity of the nuclear ellipsoid and amplitude of vibrations violating the axial symmetry. It is interesting to mention that a rather constant behavior of this quantity was found [37] to characterize the ground state of wide number of stable even-even nuclei with masses ranging from $A = 90$ to $A = 190$. The probability distributions of the 0_2^+ state [Fig. 6(b)] contain two components. One of them is similar to that of the ground-state distribution but is “compressed” by a second component centered at $\beta \approx 0.25$ and $\gamma \approx 30^\circ$. The two components approach each other with increasing mass number A . The evolution of the probability distribution of the 0_2^+ state follows closely via its first component that of the 0_1^+ state whereas the second component does not undergo special changes beside differences in the slope and some shift of peak position.

In this way, the 0_2^+ states as described by the present GCM calculations can be associated with an excitation related to the γ degree of freedom. In terms of the phonon (boson) language, they can be considered to arise from the coupling of the elementary quadrupole phonons (d bosons) in triplets. This picture is in a nice qualitative agreement with the recently [18] proposed new view of the O(6) excitations as multiple quadrupole “phonon” excitations built on the ground state. In $^{124-128}\text{Ba}$, however, the structure of these states is influenced by the details in the structure of the PES.

To conclude this section, in our opinion the GCM gives a good overall description of the properties of the excited states in $^{124-130}\text{Ba}$. In the case of ^{132}Ba , complementary experimental information is needed in order to obtain more reliable results. With respect to the energetics of the ground state and γ bands, this systematic description is better than the results of other models applied in that mass region in the past. (For specific nuclei, however, calculations exist which give a description of about the same quality.) Strong $B(E2)$ transition strengths as well as branching ratios for such transitions are also reproduced better (or at least in a comparable way). An advanced ansatz for the collective $E2$ operator can help solving problems associated with some relatively weak

transitions which are better reproduced by other models. However, more realistic potentials may also be necessary for the solution of these problems and for improving the description of the low-lying 0_2^+ states in the nuclei investigated. On the other hand, as far as the basic trends of the shape evolution are reflected by the PES derived, the GCM provides an information which is either schematically present in the output of some of the collective models considered or wanted as input data by the rest of them. One may argue that the price one has to pay for this advantage in particular and for the good overall description in general is the use of a relatively large number of parameters (eight in the present version of the GCM). In comparison, an acceptable description of the nuclei in the $A \approx 130$ mass region can be obtained with fewer (2–3) parameters by the IBA, especially in cases where the nuclei investigated reveal features which are very close to the O(6) limit. As already discussed in Sec. II A, complementary physical information on the expected potentials can considerably restrict the freedom in varying the eight parameters of the GCM. Hence the actual number of free parameters is smaller in such cases. On the other hand, the simple observation of a microscopically derived potential like the one derived by the HF+BCS calculations [41] for ^{128}Ba (Fig. 1 in the quoted work) suggest that the

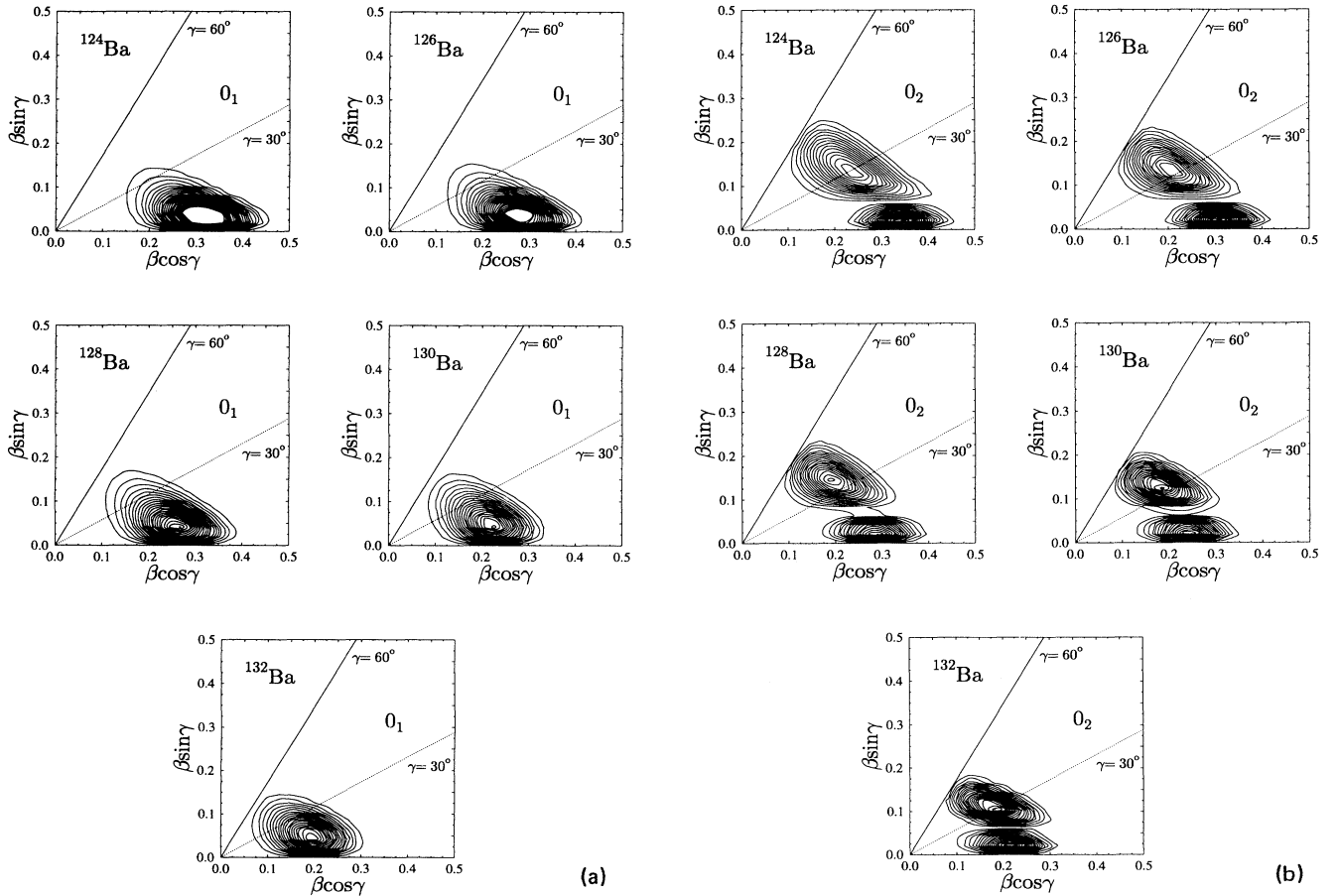


FIG. 6. (a) Probability distribution $\Psi^2 \beta^4 \sin(3\gamma)$ in the β - γ plane of the 0_1^+ wave function Ψ in $^{124-132}\text{Ba}$ [cf. Eq. (4) with $I = 0$ and $K = 0$] in $^{124-132}\text{Ba}$. (b) The same for the 0_2^+ states.

six parameters of the GCM potential may be not enough to reproduce the details. Thus, one has to accept the inconvenience of having more model parameters if the aim of a study is to obtain direct information on the nuclear shape described by the collective potential $V(\beta, \gamma)$. When essential spectroscopic experimental data are missing and no special physical restrictions can be imposed on the potentials, however, a larger number of parameters does not necessarily lead to a better description (cf. case of ^{132}Ba in Sec. II B). Correspondingly, simpler models are suitable to reveal the basic trends of the quadrupole collectivity hidden in the spectroscopic data. From this point of view, the establishment of more quantitative relations between the GCM and the IBA applied to the transitional $A \approx 130$ nuclei seems to be of general interest. This topic is considered in the next section.

B. Structure of the wave functions

In principle, the structure of the GCM wave functions with respect to ν (number of quadrupole phonons), λ (number of phonons which are not coupled pairwise to angular momentum $L=0$ or phonon seniority) and μ (number of phonon triplets coupled to $L=0$) can be used for both classification of the excited states and comparison with other collective models. However, the basis $|\nu\lambda\mu IM\rangle$ includes a large number of states which rapidly increases with the increase of the maximum number of phonons $N_{\text{ph}}^{\text{max}}$ and spin I . For example, $N_{\text{ph}}^{\text{max}} = 30$ implies a basis consisting of 91 and 304 states of spins $I^\pi = 0^+$ and $I^\pi = 8^+$, respectively. The potentials derived in the present work differ significantly from that of the quadrupole oscillator in five dimensions. Hence a large number of components participate in the building-up of the wave functions. A case where few (2–3) components dominate was not found. Normally, more than 5–6 components have appreciable contributions. In Fig. 7, the wave functions of the 0_1^+ , 2_1^+ , 2_2^+ , and 0_2^+ states in ^{128}Ba are presented in terms of the frequency distributions of the quantum numbers ν , λ , and μ [cf. Eq. (7)]. These three distributions obviously display different degrees of complexity with respect to the number and relative weights of the appreciable components in the wave functions of the different states. Thus, the structure with respect to the quantum number μ (as expressed by F_μ on the bottom of the figure) is much more simpler than the corresponding structure in ν (expressed by F_ν on the top of the figure). In the former case, most of the distributions F_μ of the low-lying states nearly overlap whereas that of the 0_2^+ state clearly deviates from the common trend (the same holds for the other members of the 0_2^+ band). Therefore, the distribution of the quantum number μ seems to be appropriate in investigating the structure of the GCM wave functions for (large-scale) classification purposes in a nucleus like ^{128}Ba .

Because of the close relationship between the basis used in the present version of the GCM and the U(5) basis used in the IBA [they coincide in the case of very large ($N \rightarrow \infty$) number of bosons] one can establish correspondences between the quantum numbers used in both

models. This is especially simple if one considers the quantum numbers labeling the basis functions in the U(5) and O(6) limits of the IBA. The analogy reads

$$\begin{array}{ccc} \text{GCM} & \text{U(5)} & \text{O(6)} \\ \nu & n_d & \\ \lambda & v & \tau \\ \mu & \tilde{n}_\Delta & \tilde{\nu}_\Delta \end{array}$$

This means, for instance, that ν can be associated with the number of d bosons n_d in the U(5) limit, etc. However, the existence of s bosons and the finite boson number N ($N = n_d + n_s$) in the IBA makes less straightforward the full equivalence. As it was shown by Moshinsky [51], a restricted version of the GCM [without the P_3 term in the kinetic energy and the term quadratic in $\cos(3\gamma)$] can be made with a suitable choice of the Hamiltonian parameters completely equivalent to the SU(3) or U(5) limiting cases of the IBA. In the general case of transitional nuclei, there are not specific formulas relating the wave functions and quantities calculated in both

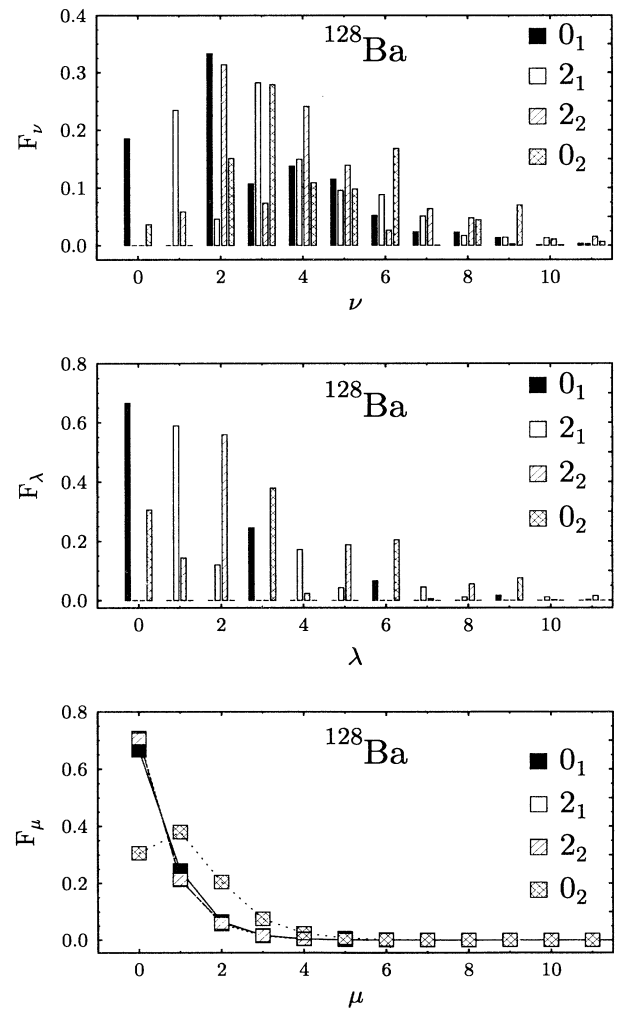


FIG. 7. Frequency distributions of the quantum numbers ν , λ , and μ characterizing the wave functions of the theoretical 0_1^+ , 2_1^+ , and 2_2^+ states in ^{128}Ba .

models. Nevertheless, the above analogies are useful for establishing concrete relations between the nuclear structure pictures proposed by the GCM and IBA in complex situations. Thus, the F_λ distribution in Fig. 7 (middle) can be interpreted as an example of perturbation of the pure O(6) limit in the case of ^{128}Ba expressed by the violation of the quantum number $\tau (= \lambda)$. In the unperturbed case, the 0_1^+ , 2_1^+ , and 2_2^+ states would belong to the multiplets characterized by $\tau=0, 1$, and 2 , respectively. According to the GCM calculation, this is realized to about 60%. Similarly, the lowest family of states (i.e., the g.s.b., γ band, etc.) in the O(6) limit consists of τ multiplets characterized by $\sigma = N$ and $\tilde{\nu}_\Delta=0$. In the GCM picture, the distribution of the analog of $\tilde{\nu}_\Delta$ (i.e., μ) points that this is valid to about 70% (Fig. 7, bottom). An interesting feature arises, however, namely that the μ distributions of most of the low-lying states are nearly the same.

In Fig. 8, the mean values of the quantum numbers ν and μ characterizing different states are plotted versus mass number A [cf. Eq. (8)]. As Fig. 7 suggests, these distributions have significant dispersions. Nevertheless, the mean values (ν) and (μ) exhibit a systematic behavior and can be used as an illustration of the changes in the structure of the wave functions due to the shape evolution occurring from ^{124}Ba to ^{132}Ba . On the top of Fig. 8, the mean $\langle \nu \rangle$ values characterizing the 0_1^+ , 2_1^+ , 2_2^+ , and 0_2^+ states are displayed. Since the $\langle \nu(0_1) \rangle$ data and the line $N=n_d+n_s$ are nearly parallel in the range from ^{124}Ba to ^{130}Ba , their constant difference can be interpreted in terms of the IBA as corresponding to a condensate of 5 s bosons present (in average) in the ground states of these nuclei. In the middle of Fig. 8, the mean number of phonons $\langle \nu \rangle$ in the g.s.b. are compared with the mean number of d bosons $\langle n_d \rangle$ expected [52] in the three limiting cases of the IBA. This comparison suggests that the nuclei investigated could be described with an IBA Hamiltonian which contains terms characteristic for an O(6)-SU(3) transitional region. Similar results implying a shape transition were obtained by Puddu *et al.* [35] in an IBA-2 calculation. We note that the figure illustrates a somewhat spin-dependent behavior of the closeness of $\langle \nu \rangle$ to the expectations of the O(6) or SU(3) limiting cases of the IBA. The already-mentioned specific behavior of the structure of the 0_2^+ wave function with respect to the number of phonon triplets coupled to $L=0$ is shown systematically in Fig. 8, bottom, by the plot of the corresponding mean values $\langle \mu \rangle$ versus mass number A . They demonstrate again the clear separation of the low-lying states into families characterized by different μ distributions. Since the separation increases towards $A \geq 130$ and $\langle \mu(0_2^+) \rangle$ keeps its value of about 1, the 0_2^+ state can be interpreted as a $\tilde{\nu}_\Delta = 1$ state in the O(6) limit of the IBA.

V. SUMMARY AND CONCLUSIONS

The generalized collective model (GCM) is able to give a reasonable description of the properties of positive-parity low-lying collective excitations in the $^{124-130}\text{Ba}$

nuclei. New data and careful identification of the collective states in ^{132}Ba and heavier isotopes are needed for an extension of the systematics. A good description of the ground-state and γ bands is obtained. In particular, a solution of the problem of the evolution of the staggering in the γ band is proposed. The GCM is able to describe also the gross features of the quadrupole properties of the investigated nuclei including absolute $B(E2)$ reduced transition probabilities and (as far as a comparison with experiment is possible) quadrupole moments. However, there are discrepancies in the description of relatively weak $E2$ transitions due to cancellation in the matrix elements which indicate, as already pointed

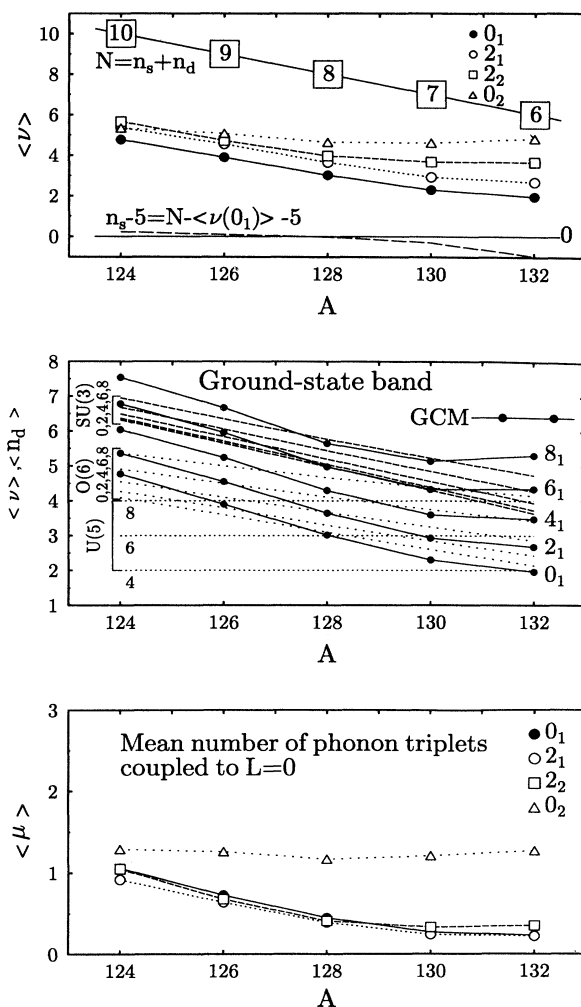


FIG. 8. Top: Mean values of the quantum number ν characterizing the wave functions of the calculated 0_1^+ , 2_1^+ , 2_2^+ , and 0_2^+ states vs mass number A . In addition, the total number of IBA-1 bosons $N = n_d + n_s$ is shown. Middle: Mean number of phonons $\langle \nu \rangle$ characterizing states of the ground-state bands (labeled by spin I). The GCM results are compared to the mean number $\langle n_d \rangle$ of d bosons calculated for the same states in the three limiting cases of the IBA. The U(5) 0_1^+ and 2_1^+ states are not shown (they are characterized by $n_d = 0$ and $n_d = 1$, respectively). Bottom: The same as on top of the figure for the quantum number μ . See also text.

out by the authors of the model (cf., e.g., Ref. [13]) the necessity of improvements in the collective $E2$ operator $Q_{2\mu}$ of the GCM. The inclusion of terms of third order in β in $Q_{2\mu}$ does not improve the results but allowing a variable contribution of the second term $Q_{2\mu}^{(2)}$ may be able to do so. On the other hand, the description of the potential $V(\beta, \gamma)$ by polynomials in β and $\cos(3\gamma)$ could be too schematic in some realistic situations. This could be the case of potential energy surfaces (PES's) with complicated structure (more than one minimum) or β dependence which goes up slowly at large values of β compared to the dependence introduced by polynomials. Such effects might influence some $B(E2)$ values and, which seems to be more important, the description of bands like the 0_2^+ ones in the barium nuclei investigated. Although the present calculations fail to reproduce the level spacing of these bands, their interpretation as excitations related to the γ degree of freedom (and therefore reflecting the γ structure of the PES) seems to be correct.

The comparison of the PES and the shape parameters characterizing the different states shows an overall reasonable agreement with previous nuclear shape calculations based on microscopic methods. It would be interesting to parametrize microscopically calculated PES in terms of functions whose matrix elements between the basis functions of the GCM are known and thus remove part of the ambiguities related to the fitting procedure.

The problem of the mass parameters seems to be, however, not so easy to handle within such a formalism. The present calculations confirm the significant deformation (β and γ) dependence of the mass parameters in the barium isotopes investigated which was established in Ref. [8] for these γ soft nuclei. Thus, microscopically calculated potentials, mass parameters, and inertial functions are necessary for a general solution of the problem (cf., e.g., the development of numerical methods proposed in Ref. [53] as further development of the GCM). The consistent and smooth evolution of nuclear shapes and properties as obtained by the present GCM calculations in a chain of isotopes supports the capacity of the model to describe basic trends in the collective motion in $^{124-132}\text{Ba}$.

ACKNOWLEDGMENTS

The authors are indebted to A. Gelberg, R.V. Jolos, R.F. Casten, and P. von Brentano for fruitful discussions and to F. Dönau and T. Mylaeus for helping the installation of the GCM code. This work was funded by the DFG under Contract No. Br799/5-2. Two of us (P.P. and W.A.) acknowledge also the financial support of the Stabsabteilung für Internationale Zusammenarbeit Karlsruhe and the Bulgarian National Research Foundation under Contracts PH301 and PH431.

-
- [1] D. Troltenier, J.A. Maruhn, W. Greiner, V. Velazquez Aguilar, P.O. Hess, and J.H. Hamilton, *Z. Phys. A* **338**, 261 (1991).
 - [2] D. Troltenier, J.A. Maruhn, and P.O. Hess, in *Computational Nuclear Physics*, edited by K. Langanke, J.A. Maruhn, and S.E. Koonin (Springer, Berlin, 1991), p. 105.
 - [3] G. Gneuss and W. Greiner, *Nucl. Phys.* **171**, 449 (1971).
 - [4] A. Arima and F. Iachello, *Ann. Phys. (N.Y.)* **123**, 469 (1979).
 - [5] R.F. Casten and P. von Brentano, *Phys. Lett.* **152B**, 22 (1985).
 - [6] J. Meyer-Ter-Vehn, *Phys. Lett.* **84B**, 10 (1979).
 - [7] L. Wilets and M. Jean, *Phys. Rev.* **102**, 788 (1956).
 - [8] S.G. Rohozinski, J. Dobaczewski, B. Nerlo-Pomorska, K. Pomorski, and J. Srebrny, *Nucl. Phys.* **A292**, 66 (1977); S.G. Rohozinski, J. Dobaczewski, B. Nerlo-Pomorska, K. Pomorski, and J. Srebrny, *Microscopic Dynamic Calculations of Collective States in Xenon and Barium Isotopes (II)* (Warsaw University Press, Warsaw, 1977).
 - [9] J. Dobaczewski and J. Skalski, *Phys. Rev. C* **40**, 1025 (1989).
 - [10] D. Habs, H. Klewe-Nebenius, K. Wisshak, R. Löhken, G. Nowicki, and H. Rebel, *Z. Phys.* **267**, 149 (1974).
 - [11] A. Arima and F. Iachello, *Ann. Phys. (N.Y.)* **99**, 253 (1976).
 - [12] A. Arima and F. Iachello, *Ann. Phys. (N.Y.)* **111**, 201 (1978).
 - [13] P.O. Hess, J.A. Maruhn, and W. Greiner, *J. Phys. G* **7**, 737 (1981).
 - [14] D. Troltenier, Frankfurt am Main Report No. GSI-92-15 1992.
 - [15] A. Bohr and B.R. Mottelson, *Nuclear Structure* (Benjamin, Reading, MA, 1975), Vol. 2.
 - [16] M. Sakai, in *Problems of Vibrational Nuclei*, edited by G. Alaga, V. Paar, and L. Sips (North-Holland, Amsterdam, 1975), p. 181.
 - [17] P. von Brentano, A. Dewald, A. Gelberg, P. Sala, I. Wiedenhöver, R. Wirowski, and J. Yan (unpublished).
 - [18] G. Siems, U. Neuneyer, I. Wiedenhöver, S. Albers, M. Eschenauer, R. Wirowski, A. Gelberg, P. von Brentano, and T. Otsuka, *Phys. Lett. B* **320**, 1 (1994).
 - [19] N. Idrissi, A. Gizon, J. Genevey, P. Paris, V. Barci, D. Barnéoud, J. Blachot, D. Bucurescu, R. Duffait, J. Gizon, C.F. Liang, and B. Weiss, *Z. Phys. A* **341**, 427 (1992).
 - [20] S. Pilotte, S. Flibotte, S. Monaro, N. Nadon, D. Prévost, P. Taras, H.R. Andrews, D. Horn, V.P. Janzen, D.C. Radford, D. Ward, J.K. Johansson, J.C. Waddington, T.E. Drake, and A. Galindo-Uribarri, *Nucl. Phys.* **A514**, 545 (1990).
 - [21] K. Schiffer, A. Dewald, A. Gelberg, R. Reinhardt, K.O. Zell, S. Xianfu, and P. von Brentano, *Z. Phys. A* **327**, 251 (1987).
 - [22] G. Siems, Ph.D. thesis, University of Köln, 1993.
 - [23] K. Schiffer, A. Dewald, A. Gelberg, R. Reinhardt, K.O. Zell, S. Xianfu, and P. von Brentano, *Nucl. Phys.* **A458**, 337 (1986).
 - [24] S. Xianfu, D. Bazacco, W. Gast, A. Gelberg, U. Kaup, K. Schiffer, A. Dewald, R. Reinhardt, K.O. Zell, and P. von Brentano, *Nucl. Phys.* **A436**, 506 (1985).
 - [25] Y.V. Sergeenkov, *Nucl. Data Sheets* **65**, 277 (1992).
 - [26] E.S. Paul, D.B. Fossan, Y. Liang, R. Ma, and N. Xu, *Phys. Rev. C* **40**, 1255 (1989).
 - [27] S.G. Rohozinski, J. Srebrny, and K. Horbaczewska, *Z.*

- Phys. **268**, 401 (1974).
- [28] A. Dewald, P. Petkov, R. Wrzal, G. Siems, R. Wirowski, P. Sala, G. Böhm, A. Gelberg, K.O. Zell, P. von Brentano, P.J. Nolan, A.J. Kirwan, D.J. Bishop, R. Julin, A. Lampinen, and J. Hattula, in *Selected Topics in Nuclear Structure*, Proceedings of the XXV Zakopane School on Physics, edited by J. Styczeń and Z. Stachura (World Scientific, Singapore, 1990), Vol. 2, p. 152.
- [29] P. Sala *et al.*, unpublished; P. Sala, Ph.D. thesis, University of Köln, 1993.
- [30] K. Schiffer, S. Harissopulos, A. Dewald, A. Gelberg, K.O. Zell, P. von Brentano, P.J. Nolan, A. Kirwan, D.J.G. Love, D.J. Thornley, and P.J. Bishop, *J. Phys. G* **15**, L85 (1989).
- [31] P. Petkov, S. Harissopulos, A. Dewald, M. Stolzenwald, G. Böhm, P. Sala, K. Schiffer, A. Gelberg, K.O. Zell, P. von Brentano, and W. Andrejtscheff, *Nucl. Phys.* **A543**, 589 (1992).
- [32] G. Böhm, Ph.D. thesis, University of Köln, 1991.
- [33] A. Dewald (unpublished).
- [34] S.M. Burnett, A.M. Baxter, G.J. Gyapong, M.P. Fewell, and R.H. Spear, *Nucl. Phys.* **A494**, 102 (1989).
- [35] G. Puddu, O. Scholten, and T. Otsuka, *Nucl. Phys.* **A348**, 109 (1980).
- [36] J.M. Eisenberg and W. Greiner, *Nuclear Models* (North-Holland, Amsterdam, 1987).
- [37] W. Andrejtscheff and P. Petkov, *Phys. Rev. C* **48**, 2531 (1993).
- [38] V.M. Strutinsky, *Nucl. Phys.* **A95**, 420 (1967).
- [39] I. Ragnarsson, A. Sobiczewski, R.K. Sheline, S.E. Larsson, and B. Nerlo-Pomorska, *Nucl. Phys.* **A233**, 329 (1974).
- [40] B.D. Kern, R.L. Mlekodaj, G.A. Leander, M.O. Kortelathi, E.F. Zganjar, R.A. Braga, R.W. Fink, C.P. Perez, W. Nazarewicz, and P.B. Semmes, *Phys. Rev. C* **36**, 1515 (1987).
- [41] A. Coc, P. Bonche, H. Flocard, and P.H. Heenen, *Phys. Lett. B* **192**, 263 (1987).
- [42] P. Möller, J.R. Nix, W.D. Mayers, and W.J. Swiatecki, unpublished.
- [43] R. Wyss, private communication.
- [44] J. Ginocchio and M. Kirson, *Nucl. Phys.* **A350**, 31 (1980).
- [45] T. Komatsubara, T. Hosoda, H. Sakamoto, T. Aoki, and K. Furuno, *Nucl. Phys.* **A496**, 605 (1989).
- [46] R.F. Casten, P. von Brentano, K. Heyde, P. Van Isacker, and J. Jolie, *Nucl. Phys.* **A439**, 289 (1985).
- [47] A. Sevrin, K. Heyde, and J. Jolie, *Phys. Rev. C* **36**, 2621 (1987).
- [48] A. Novoselsky and I. Talmi, *Phys. Lett. B* **172**, 139 (1986).
- [49] H.G. Solari, R. Gilmore, and M. Vallieres, *Phys. Rev. C* **35**, 320 (1987).
- [50] W. Lieberz, A. Dewald, W. Frank, A. Gelberg, W. Krips, D. Lieberz, R. Wirowski, and P. von Brentano, *Phys. Lett. B* **240**, 38 (1990).
- [51] M. Moshinsky, *Nucl. Phys.* **A338**, 156 (1980).
- [52] F. Iachello and A. Arima, *The Interacting Boson Model* (Cambridge University Press, Cambridge, 1987).
- [53] D. Troltenier, J.A. Maruhn, W. Greiner, and P.O. Hess, *Z. Phys. A* **343**, 25 (1992).